VISER
www.viserdata.com

# RESEARCH AND APPLICATION OF MATERIALS SCIENCE

ISSN 2661-4464(online) 2661-4456(print)
Volume 8 No. 1 2026

# COMPANY INTRODUCTION

Viser Technology Pte. Ltd. was founded in Singapore with branch offices in both Hebei and Chongqing, China. Viser focuses on publishing scientific and technological journals and books that promote the exchange of scientific and technological findings among the research community and around the globe. Despite being a young company, Viser is actively connecting with well-known universities, research institutes, and indexation database, and has already established a stable collaborative relationship with them. We also have a group of experienced editors and publishing experts who are dedicated to publishing high-quality journal and book contents. We offer the scholars various academic journals covering a variety of subjects and we are committed to reducing the hassles of scholarly publishing. To achieve this goal, we provide scholars with an all-in-one platform that offers solutions to every publishing process that a scholar needs to go through in order to show their latest finding to the world.

# Research and Application of Materials Science



**Publisher:** Viser Technology Pte. Ltd.

**ISSN:** 2661-4464(online)
2661-4456(print)

**Frequency:** Semi-annual

**Add.:** 195 Pearl's Hill Terrace, #02-41,
Singapore 168976

**https://www.viserdata.com/**

*Research and Application of Materials Science*

**Volume 8 No.1 (2026)**

## CONTENTS

**Performance of Low-Carbon Mortar Prepared with $CO_2$-Carbonated Carbide Slag as a Partial Cement Substitute**

Chao LIU, Chao YANG, Chao ZHU ..... 1

**Simulation Study on the Mixing Process of Polydimethylsiloxane/Carbon Fiber Composites**

Wenkai ZHOU, Xiaoxiang HE ..... 9

**Preparation and Performance Regulation of Carbon-Fiber-Reinforced PC/ABS Composites for Microwave Absorption and EMI Shielding**

WenTao YU, Jichao DING, Liting HAO, Lulin WANG, Yeming XIAN ..... 14

**Direct $CO_2$ Capture by Carbide Slag: Moisture Regulation, Uptake Performance, and Reaction Kinetics**

Chao LIU, Chao YANG, Chao ZHU ..... 21

Viser Technology Pte. Ltd.
Research and Application of Materials Science
DOI: 10.33142/rams.v8i1.20144

Research Article Open Access

# Performance of Low-Carbon Mortar Prepared with $CO_2$-Carbonated Carbide Slag as a Partial Cement Substitute

**Chao LIU*, Chao YANG, Chao ZHU**

Xi'an University of Architecture and Technology, Xi'an, Shanxi, 710055, China

*Corresponding Author: CHao LIU, E-mail:chaoliu@xauat.edu.cn

**Abstract**

To explore the feasibility of using $CO_2$-carbonated carbide slag in low-carbon cementitious materials, this study investigated the basic properties of raw carbide slag and $CO_2$-carbonated carbide slag, and further used $CO_2$-carbonated carbide slag as a partial cement substitute to prepare low-carbon mortar. Five replacement ratios of $CO_2$-carbonated carbide slag, namely 0%, 5%, 10%, 15% and 20%, were designed to evaluate their effects on mortar flowability, compressive strength, water absorption, bulk density, leaching pH and $Ca^{2+}$ release behavior. The results showed that $CO_2$ carbonation increased the $CaCO_3$ content of carbide slag from 4.0 wt.% to 41.6 wt.%, decreased the $Ca(OH)_2$ content from 92.0 wt.% to 48.2 wt.%, and reduced the pH from 12.60 to 10.55, indicating that carbonation can reduce alkalinity and form carbonate-rich products. When the replacement ratios of $CO_2$-carbonated carbide slag were 5% and 10%, the 28-day compressive strengths of mortar were 50.2 MPa and 49.6 MPa, respectively, slightly higher than that of the control group (48.5 MPa). When the replacement ratio increased to 20%, the 28-day compressive strength decreased to 41.3 MPa. The water absorption and bulk density results indicated that 5%-10% replacement was beneficial to improving mortar compactness, whereas excessive replacement weakened the dense structure. Leaching tests showed that the leachate pH and $Ca^{2+}$ concentration slightly decreased with increasing replacement ratio, suggesting that $CO_2$-carbonated carbide slag did not increase the risk of alkaline release. Overall, $CO_2$-carbonated carbide slag can be used as a partial cement substitute in low-carbon mortar, and a replacement ratio of 5%-10% is considered suitable.

***Keywords:*** *carbide slag; $CO_2$ carbonation; low-carbon mortar; cement replacement; compressive strength; environmental compatibility*

## 1 Introduction

With increasing demand for carbon reduction in the construction materials sector, the utilization of industrial solid wastes for low-carbon cementitious materials has attracted growing attention. Carbide slag is a large-volume alkaline industrial by-product generated during acetylene production by calcium carbide hydrolysis. It is mainly composed of $Ca(OH)_2$ and contains small amounts of $CaCO_3$, $CaO$, $SiO_2$, $Al_2O_3$, $Fe_2O_3$ and $MgO$[1-6]. Due to its strong alkalinity and relatively high moisture content, long-term stockpiling of carbide slag may cause land occupation, dust emission and alkaline leachate problems. However, the abundant $Ca(OH)_2$ in carbide slag also gives it high reactivity toward $CO_2$, allowing it to generate $CaCO_3$ through carbonation, reduce material alkalinity and achieve $CO_2$ mineral fixation[7,8].

Previous studies have shown that carbide slag can be used in $CO_2$ mineralization, alkali-activated cementitious materials and construction materials[1,2,4,9-11]. Nevertheless, raw carbide slag has strong alkalinity and variable composition, and its direct incorporation into cement-based materials may affect workability, pore structure and environmental safety[9,11,12]. After $CO_2$ carbonation, part of the $Ca(OH)_2$ in carbide slag is converted into $CaCO_3$, resulting in lower alkalinity. Meanwhile, the generated $CaCO_3$ fine particles may act as fillers and nucleation sites in cement-based systems[13,14]. Therefore, $CO_2$-carbonated carbide slag has potential as a partial cement replacement component



Received: March 7, 2026; Accepted: April 20, 2026

in low-carbon mortar.

However, $CO_2$-carbonated carbide slag has limited intrinsic cementitious activity, and its replacement ratio should be carefully controlled. Moderate incorporation may improve particle packing and matrix compactness, whereas excessive cement replacement may reduce the effective clinker content, decrease hydration product formation and weaken mortar strength[14,15]. In addition, whether the incorporation of carbonated carbide slag affects alkaline release or $Ca^{2+}$ leaching requires further evaluation[8,12,16]. In this study, $CO_2$-carbonated carbide slag was used as a partial cement substitute to prepare low-carbon mortar with different replacement ratios. The workability, compressive strength, water absorption, bulk density and leaching behavior of the mortars were systematically analyzed to preliminarily evaluate the feasibility of using $CO_2$-carbonated carbide slag in low-carbon cementitious materials.

## 2 Materials and Methods

### 2.1 Raw materials and preparation of $CO_2$ -carbonated carbide slag

The carbide slag used in this study was an industrial by-product generated during acetylene production by calcium carbide hydrolysis and is denoted as CS. Before testing, the raw carbide slag was dried in an oven at 105 ℃ to constant mass, followed by grinding and sieving to obtain a dried carbide slag powder with relatively uniform particle distribution. The raw carbide slag had strong alkalinity, with a pH of approximately 12.60, a $Ca(OH)_2$ content of approximately 92.0 wt.% and a $CaCO_3$ content of approximately 4.0 wt.%.

The $CO_2$-carbonated carbide slag is denoted as CCS. Based on the previous direct carbonation results of carbide slag, the optimized carbonation condition was adopted to prepare CCS. Specifically, the moisture content was adjusted to 20% on the basis of dried carbide slag, and $CO_2$ was introduced under ambient temperature and pressure for direct carbonation for 120 min. After carbonation, the samples were sealed and stored for subsequent use. Ordinary Portland cement was used as the basic cementitious material, standard sand was used as fine aggregate, and tap water or deionized water was used for mixing.

### 2.2 Mortar mix proportions and specimen preparation

To investigate the effect of CCS replacement ratio on mortar performance, five replacement ratios of 0%, 5%, 10%, 15% and 20% were designed. The 0% group was used as the ordinary cement mortar control group and denoted as M0; the other groups were denoted as M5, M10, M15 and M20, respectively. The water-to-binder ratio of all mortars was fixed at 0.50, and the binder-to-sand ratio was fixed at 1:3. The total binder mass was 450 g, the standard sand mass was 1350 g, and the mixing water mass was 225 g. This mix design was based on commonly used cement mortar testing proportions and allowed comparison of the effect of different cement replacement ratios on mortar performance[17]. The detailed mix proportions are shown in Table 1.

During mixing, cement, CCS and standard sand were first dry-mixed uniformly. Mixing water was then added, and stirring continued until a homogeneous mortar was obtained. The fresh mortar was placed into molds, compacted by vibration and then cured under standard curing conditions to ages of 3, 7 and 28 days. If standard mortar prisms are used, specimens of 40 mm × 40 mm × 160 mm can be adopted; if cubic specimens are used, the specimen size and loading method should be clearly specified in the experimental section.

**Table 1** Mix proportions of mortars with different CCS replacement ratios.

| Group | CCS replacement ratio (%) | Cement (g) | CCS (g) | Standard sand (g) | Water (g) | Water-to-binder ratio |
|---|---|---|---|---|---|---|
| M0 | 0 | 450.0 | 0 | 1350 | 225 | 0.50 |
| M5 | 5 | 427.5 | 22.5 | 1350 | 225 | 0.50 |
| M10 | 10 | 405.0 | 45.0 | 1350 | 225 | 0.50 |
| M15 | 15 | 382.5 | 67.5 | 1350 | 225 | 0.50 |
| M20 | 20 | 360.0 | 90.0 | 1350 | 225 | 0.50 |

### 2.3 Testing methods

The basic properties of CS and CCS were characterized by pH measurement, X-ray diffraction (XRD) and thermogravimetry/differential thermogravimetry (TG/DTG) to evaluate the effect of $CO_2$ carbonation on alkalinity and phase composition. XRD was used to analyze the characteristic peaks of $Ca(OH)_2$ and $CaCO_3$, whereas TG/DTG was used to estimate the contents of $CaCO_3$ and $Ca(OH)_2$.

The flowability of fresh mortar was measured to evaluate the effect of cement replacement by CCS on workability. Compressive strength tests were performed at curing ages of 3, 7 and 28 days. At least three parallel specimens were tested for each group, and the average value was used as the final result. After 28 days, water absorption and bulk density were measured. The water absorption was calculated using the following equation:

$$W_a = \frac{m_s - m_d}{m_d} \times 100\% \quad (1)$$

Where $W_a$ is the water absorption, $m_d$ is the dry mass of the specimen, and $m_s$ is the saturated mass after water absorption.

To evaluate the alkaline release of mortar containing CCS, 28-day mortar specimens were crushed and immersed at a fixed liquid-to-solid ratio. The leachate pH and $Ca^{2+}$ concentration were then measured. The 28-day strength retention was calculated as follows:

$$R_f = \frac{f_i}{f_o} \times 100\% \quad (2)$$

Where $R_f$ is the 28-day strength retention, $f_i$ is the 28-day compressive strength of mortar with a given CCS replacement ratio, and $f_o$ is the 28-day compressive strength of the control group M0. The overall experimental workflow is shown in Figure 1.

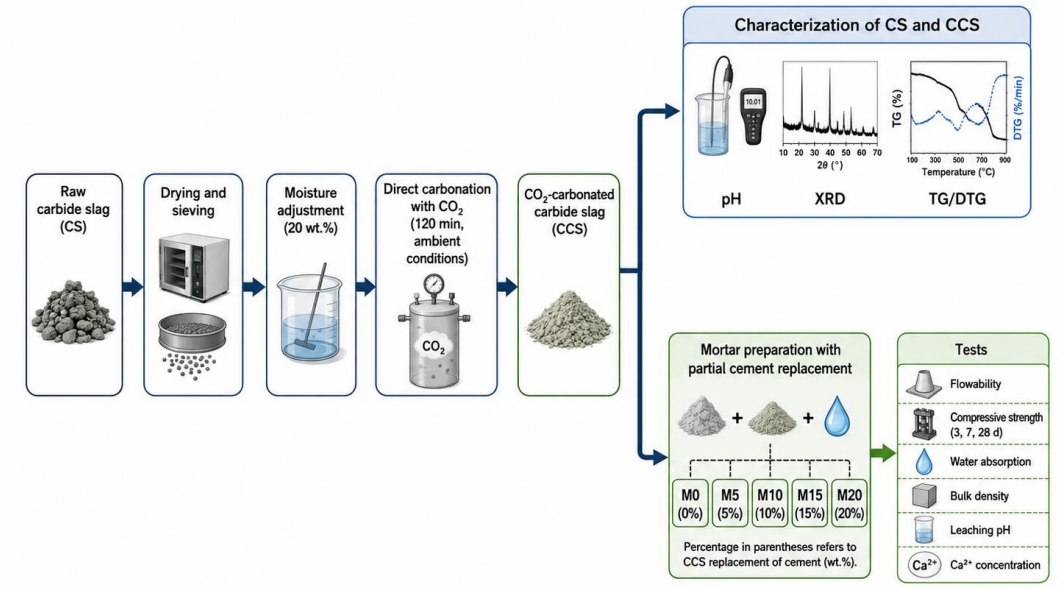


**Figure 1** Experimental workflow for preparing low-carbon mortar with $CO_2$-carbonated carbide slag

## 3 Results and Discussion

### 3.1 Comparison of basic properties between CS and CCS

The basic properties of CS and CCS are listed in Table 2, and the related characterization results are shown in Figure 2. The raw carbide slag (CS) showed strong alkalinity, with a pH of 12.60, a $Ca(OH)_2$ content of 92.0 wt.% and a $CaCO_3$ content of only 4.0 wt.%. After $CO_2$ carbonation, the pH of CCS decreased to 10.55, the $CaCO_3$ content increased to 41.6 wt.%, and the $Ca(OH)_2$ content decreased to 48.2 wt.%. These results indicate that $CO_2$ carbonation promoted the conversion of $Ca(OH)_2$ into $CaCO_3$ and effectively reduced the strong alkalinity of carbide slag.

**Table 2** Comparison of basic properties between CS and CCS.

| Sample | pH | $CaCO_3$ content (wt.%) | $Ca(OH)_2$ content (wt.%) |
|---|---|---|---|
| CS | 12.60 | 4.0 | 92.0 |
| CCS | 10.55 | 41.6 | 48.2 |

The XRD results further confirmed the phase changes before and after carbonation. CS exhibited strong characteristic peaks of $Ca(OH)_2$ and weak peaks of $CaCO_3$. After carbonation, the $CaCO_3$ peaks in CCS were enhanced, whereas the $Ca(OH)_2$ peaks were weakened. TG/DTG results also showed increased mass

loss in the $CaCO_3$ decomposition region and decreased mass loss associated with $Ca(OH)_2$ dehydration. These results indicate that $CO_2$ reacted with $Ca(OH)_2$ in carbide slag and generated considerable $CaCO_3$. Compared with raw carbide slag, CCS had lower alkalinity and higher carbonate content, making it more suitable as a substitute component in low-carbon cementitious materials.

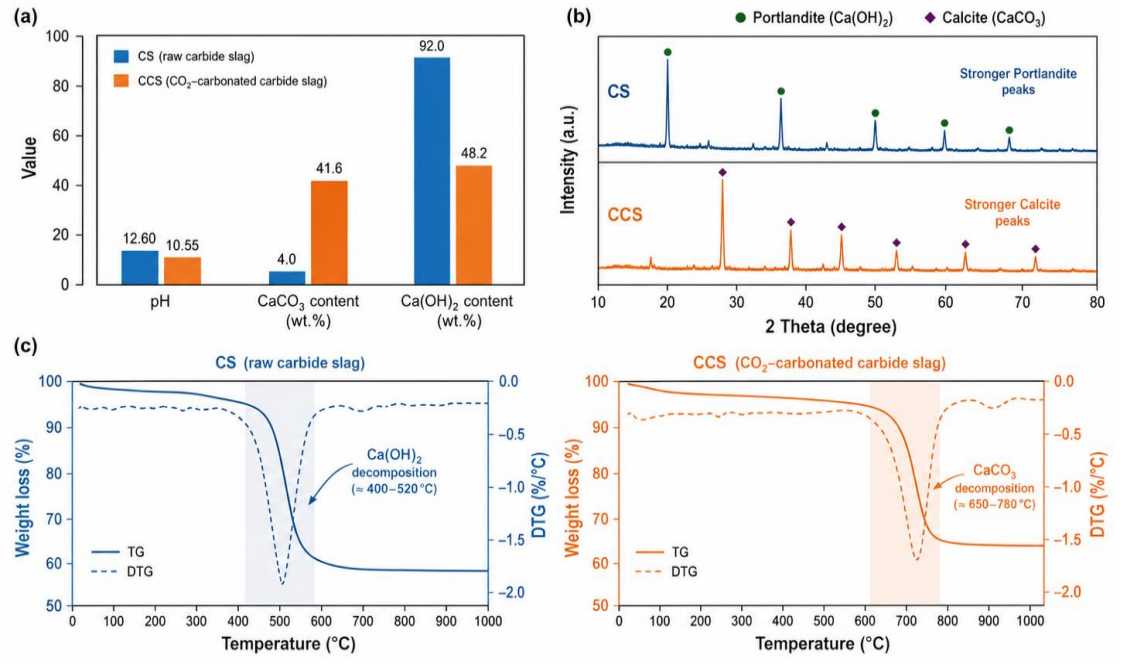


**Figure 2** Comparison of basic properties between raw carbide slag (CS) and $CO_2$-carbonated carbide slag (CCS). (a) Basic properties; (b) XRD patterns ;(c) TG/DTG curves

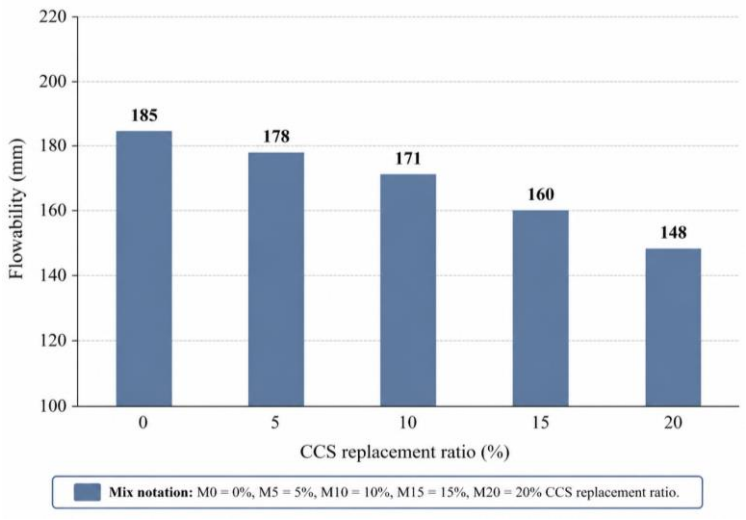


**Figure 3** Flowability of mortars with different CCS replacement ratios

### 3.2 Effect of CCS replacement ratio on mortar flowability

The flowability of mortars with different CCS replacement ratios is shown in Table 3 and Figure 3. The flowability of the M0 group was 185 mm. As the CCS replacement ratio increased, mortar flowability gradually decreased. The flowabilities of M5 and M10 were 178 mm and 171 mm, respectively, indicating that good workability was still maintained. When the replacement ratio increased to 15% and 20%, the flowability decreased to 160 mm and 148 mm, respectively.

**Table 3** Flowability of mortars with different CCS replacement ratios.

| CCS replacement ratio (%) | Flowability (mm) | Workability evaluation |
|---|---|---|
| 0 | 185 | Good |
| 5 | 178 | Good |
| 10 | 171 | Relatively good |
| 15 | 160 | Slightly decreased |
| 20 | 148 | Obviously decreased |

The decrease in flowability may be related to the rough surface, relatively high water absorption and altered particle grading of CCS. A small amount of CCS could maintain acceptable mixing performance, whereas a high CCS content increased internal friction in the paste and reduced mortar flowability. These results suggest that the CCS replacement ratio should not be too high when no additional water reducer is used.

### 3.3 Effect of CCS replacement ratio on mortar compressive strength

The compressive strength results of mortars with different CCS replacement ratios are shown in Table 4 and Figure 4. Overall, the CCS replacement ratio had a clear effect on mortar strength. The 28-day compressive strength of M0 was 48.5 MPa. The 28-day strengths of M5 and M10 were 50.2 MPa and 49.6 MPa, respectively, which were 3.5% and 2.3% higher than that of M0. This indicates that low CCS replacement did not negatively affect mortar strength and even slightly improved it.

**Table 4** Compressive strength of mortars with different CCS replacement ratios.

| CCS replacement ratio (%) | 3 d compressive strength (MPa) | 7 d compressive strength (MPa) | 28 d compressive strength (MPa) | 28 d strength retention (%) |
|---|---|---|---|---|
| 0 | 24.8 | 35.6 | 48.5 | 100.0 |
| 5 | 26.1 | 37.4 | 50.2 | 103.5 |
| 10 | 25.6 | 36.8 | 49.6 | 102.3 |
| 15 | 23.4 | 33.9 | 45.7 | 94.2 |
| 20 | 20.7 | 30.2 | 41.3 | 85.2 |

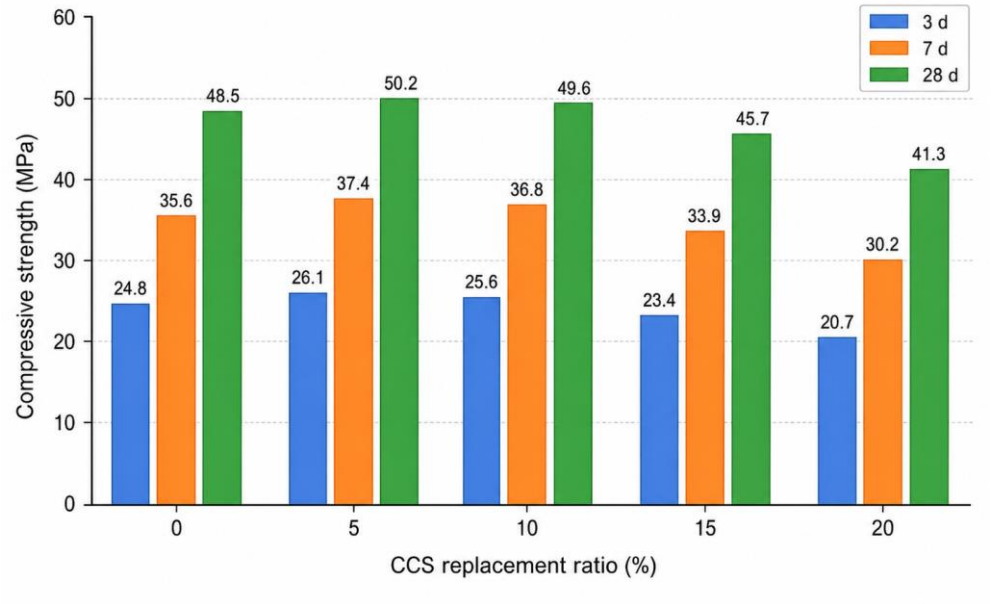


**Figure 4** Compressive strength of mortars with different CCS replacement ratios at 3, 7 and 28 days

The improvement in strength at low CCS contents may be attributed to the filling effect of $CaCO_3$ fine particles. The $CaCO_3$ particles in CCS can fill voids between cement particles, improve particle packing and provide nucleation sites for hydration products, thereby increasing mortar compactness. When the CCS replacement ratio increased to 15% and 20%, mortar strength decreased. The 28-day compressive strengths of M15 and M20 were 45.7 MPa and 41.3 MPa, respectively, with strength retention values of 94.2% and 85.2%. This indicates that CCS cannot replace cement at high ratios. Because CCS has limited cementitious activity, excessive replacement reduces the effective clinker content and decreases hydration product

formation, thereby weakening mortar strength. Therefore, from the perspective of strength, a CCS replacement ratio of 5%-10% is considered appropriate.

### 3.4 Effect of CCS replacement ratio on water absorption, density and leaching behavior

The 28-day water absorption, bulk density, leachate pH and $Ca^{2+}$ concentration of mortars with different CCS replacement ratios are shown in Table 5 and Figure 5. The M0 group had a water absorption of 7.8%, a bulk density of 2180 kg/m$^3$ and a leachate pH of 12.35. The water absorptions of M5 and M10 decreased to 7.2% and 7.4%, while their bulk densities increased to 2205 kg/m$^3$ and 2198 kg/m$^3$, respectively. This indicates that an appropriate CCS content improved mortar compactness, which is consistent with the compressive strength results.

When the CCS replacement ratio increased to 15% and 20%, the water absorption increased to 8.3% and 9.5%, respectively, while the bulk density decreased to 2165 kg/m$^3$ and 2138 kg/m$^3$. This indicates that high CCS contents increased internal porosity and made the mortar matrix relatively loose. These results further explain the strength reduction observed in the M15 and M20 groups.

The leachate pH and $Ca^{2+}$ concentration slightly decreased with increasing CCS replacement ratio. The leachate pH and $Ca^{2+}$ concentration of M20 were 11.88 and 435 mg/L, respectively, both lower than those of M0. This is mainly because part of $Ca(OH)_2$ in CCS had already been converted to $CaCO_3$ during carbonation, and its strong alkalinity and soluble calcium release capacity were lower than those of raw carbide slag. Therefore, the incorporation of CCS did not increase alkaline release from mortar; instead, it slightly reduced the leachate pH and $Ca^{2+}$ concentration.

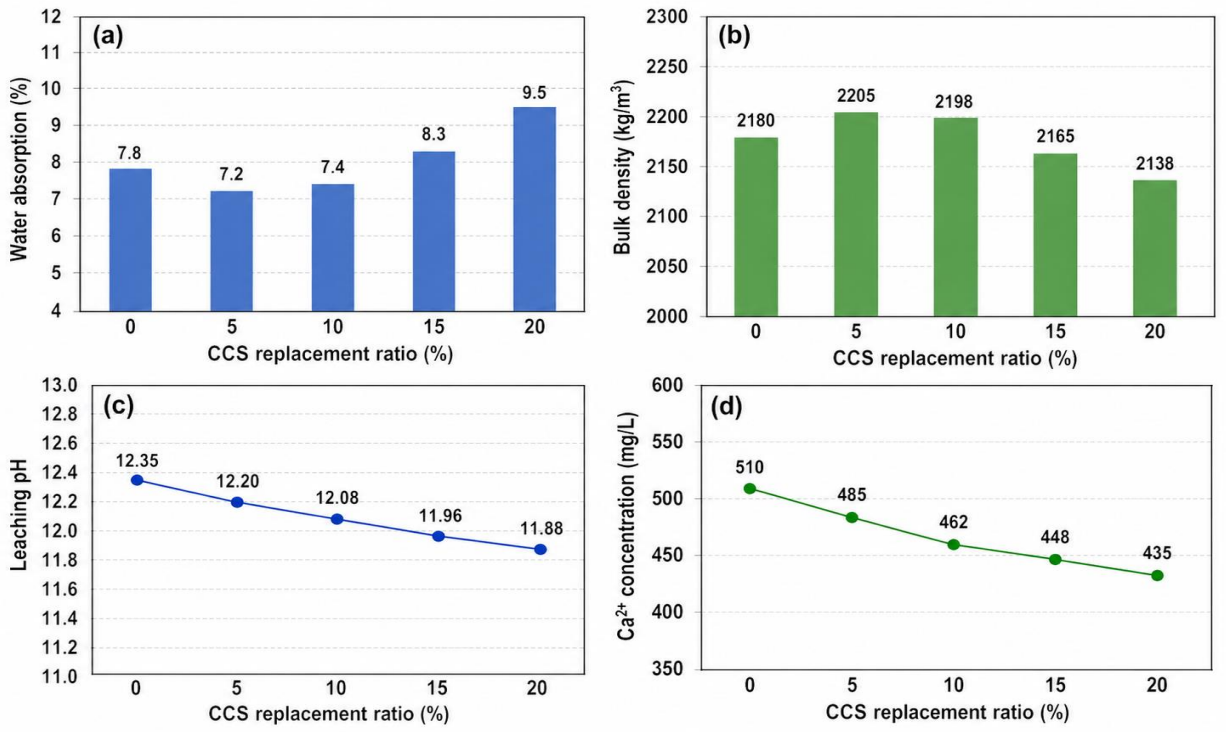


**Figure 5** Physical properties and leaching behavior of mortars with different CCS replacement ratios

**Table 5** Water absorption, bulk density and leaching results of mortars with different CCS replacement ratios.

| CCS replacement ratio (%) | 28 d water absorption (%) | Bulk density (kg·m$^{-3}$) | 28 d leachate pH | $Ca^{2+}$ concentration (mg·L$^{-1}$) |
|---|---|---|---|---|
| 0 | 7.8 | 2180 | 12.35 | 510 |
| 5 | 7.2 | 2205 | 12.20 | 485 |
| 10 | 7.4 | 2198 | 12.08 | 462 |
| 15 | 8.3 | 2165 | 11.96 | 448 |
| 20 | 9.5 | 2138 | 11.88 | 435 |

### 3.5 Overall discussion

The above results indicate that the effect of $CO_2$-carbonated carbide slag on mortar performance was strongly dosage-dependent. At CCS replacement ratios of 5%-10%, $CaCO_3$ particles in CCS provided a filling effect in the mortar, improving matrix compactness. This was reflected by a slight increase in compressive strength and a decrease or slight change in water absorption. Meanwhile, carbonation reduced the $Ca(OH)_2$ content of carbide slag, so the incorporation of CCS did not significantly increase alkaline release from mortar.

When the CCS replacement ratio further increased to 15%-20%, the cement content in the system decreased, hydration product formation was reduced and flowability declined. These effects resulted in a looser mortar structure, lower compressive strength and higher water absorption. Therefore, CCS should not be used as a high-ratio cement replacement. Considering workability, compressive strength, water absorption and leaching behavior, a replacement ratio of 5%-10% is considered a reasonable range.

## 4 Conclusions

This study investigated the feasibility of using $CO_2$-carbonated carbide slag as a partial cement substitute for preparing low-carbon mortar. The results showed that $CO_2$ carbonation significantly changed the phase composition and alkalinity of carbide slag. The $CaCO_3$ content increased from 4.0 wt.% to 41.6 wt.%, the $Ca(OH)_2$ content decreased from 92.0 wt.% to 48.2 wt.%, and the pH decreased from 12.60 to 10.55. This indicates that carbonation promoted the conversion of $Ca(OH)_2$ into $CaCO_3$ and reduced the strong alkalinity of carbide slag.

The CCS replacement ratio had a significant effect on mortar workability and compressive strength. As the CCS replacement ratio increased, mortar flowability gradually decreased. When the CCS replacement ratios were 5% and 10%, the 28-day compressive strengths were 50.2 MPa and 49.6 MPa, respectively, slightly higher than that of the control group (48.5 MPa). When the replacement ratio increased to 20%, the 28-day compressive strength decreased to 41.3 MPa. Appropriate CCS incorporation can provide a filling effect and improve mortar structure, whereas excessive CCS reduces the effective cement content and hydration product formation, thereby weakening strength.

The water absorption, bulk density and leaching results showed that 5%-10% CCS was beneficial for improving mortar compactness, whereas 15%-20% CCS increased water absorption and decreased bulk density. The leachate pH and $Ca^{2+}$ concentration slightly decreased with increasing CCS replacement ratio, indicating that CCS incorporation did not increase the risk of alkaline release. Based on strength, workability, water absorption and leaching behavior, $CO_2$-carbonated carbide slag can be used as a partial cement substitute in low-carbon mortar, with a suitable replacement ratio of 5%-10%.

**Funding:** This work was supported by the National Natural Science Foundation of China (No. 52508304), the Interdisciplinary Innovation and Enhancement Program of Xi'an University of Architecture and Technology (No. 2025JCK01).

## References

[1] WANG S, LIN X, ZHANG Y, et al. A review of utilizing carbide slag to sequestrate carbon dioxide by mineral carbonation: Mechanisms, processes, and value-added products [J]. Fuel, 2025(384): 134041.

[2] KOTHARI M S, ALY HASSAN A, EL-DIEB A, et al. Recent advancements in CO2 capture and storage using carbide slag waste: a review of technological and chemical innovations [J]. Current Opinion in Chemical Engineering, 2025(49): 101169.

[3] Direct mineral carbonation of carbide slag waste in fixed bed reactor: comparison of dry and wet route Sustainable Environment Research Springer Nature Link [EB]. [2026-06-09].

[4] YANG J, LIU S, MA L, et al. Mechanism analysis of carbide slag capture of CO2 via a gas-liquid-solid three-phase fluidization system [J]. Journal of Cleaner Production, 2021(279): 123712.

[5] Research on Utilizable Calcium from Calcium Carbide Slag with Different Extractors and Its Effect on CO2 Mineralization [EB]. [2026-06-09].

[6] GAO Y, WANG J, WEI B, et al. Understanding the mechanism of CO2 mineralization and carbon sequestration performance in carbide slag: Effects of liquid-solid ratio and gas flow rate [J]. Journal of Environmental Management, 2025(390): 126246.

[7] ZHANG W, LI Y, HE Z, et al. CO2 capture by carbide slag calcined under high-concentration steam and energy requirement in calcium looping conditions [J]. Applied Energy, 2017(206): 869-878.

[8] KOTHARI M S, MOHAMED B A, ALY HASSAN A, et al. Environmental impacts of low-temperature CO2

sequestration via carbide slag waste mineral carbonation and utilization of carbonated end-product[J]. Journal of Environmental Chemical Engineering, 2025, 13(6): 119767.

[9] BAWAB J, EL-HASSAN H, EL-DIEB A, et al. Utilization of calcium carbide residue as a concrete component: A comprehensive review [J]. Case Studies in Construction Materials, 2025(22): 04823.

[10] JULPHUNTHONG P, JOYKLAD P, MANPROM P, et al. Evaluation of calcium carbide residue and fly ash as sustainable binders for environmentally friendly loess soil stabilization [J]. Scientific Reports, 2024, 14(1): 671.

[11] Effect of Calcium Carbide Residue on Strength Development along with Mechanisms of Cement-Stabilized Dredged Sludge [EB]. [2026-06-09].

[12] Study on the Properties and Hydration Mechanism of Calcium Carbide Residue-Based Low-Carbon Cementitious Materials [EB]. [2026-06-09].

[13] BAWAB J, EL-HASSAN H, EL-DIEB A, et al. Accelerated carbonation curing of concrete incorporating calcium carbide residue[J]. Journal of Building Engineering, 2024(88): 109258.

[14] The Characterization of Carbide Slag by Carbonation Curing and Its Enhancement Performance in Blended Cement Paste Journal of Materials in Civil Engineering Vol 36, No 1[EB]. [2026-06-09].

[15] ZHENG Y, LIU C, WANG J, et al. High-dosage carbide slag-based cementitious material: Workability, mechanical strength, and carbonation behavior with the performance enhancement [J]. Case Studies in Construction Materials, 2025(23): 05145.

[16] MAKARATAT N, JATURAPITAKKUL C, NAMARAK C, et al. Effects of binder and CaCl2 contents on the strength of calcium carbide residue-fly ash concrete[J]. Cement and Concrete Composites, 2011, 33(3): 436-443.

[17] APOSTOLOPOULOU M, ARMAGHANI D J, BAKOLAS A, et al. Compressive strength of natural hydraulic lime mortars using soft computing techniques[J]. Procedia Structural Integrity, 2019(17): 914-923.

Viser Technology Pte. Ltd.
Research and Application of Materials Science
DOI: 10.33142/rams.v8i1.20145

Research Article Open Access

# Simulation Study on the Mixing Process of Polydimethylsiloxane/Carbon Fiber Composites

**Wenkai ZHOU, Xiaoxiang HE***

School of Mechanical Engineering and Mechanics, Xiangtan University, Xiangtan, Hunan, 411105, China

***Corresponding Author:** Xiaoxiang HE, E-mail: heshosha@163.com*

**Abstract**

Uniform filler dispersion is vital to form thermal networks within polymer composites. Planetary centrifugal blending enables high-quality composite fabrication, yet the microscale dispersion mechanism of carbon fiber (CF) in polydimethylsiloxane (PDMS) remains unclear. This work adopted EDEM-based discrete element simulation to explore the dispersion characteristics of CFs in PDMS during planetary centrifugal stirring. With mixing deviation as the quantitative evaluation indicator, the effects of CF loading, mixing time and mixing speed on dispersion uniformity were analyzed. The results showed that increasing CF content within 1-5 vol% improved dispersion uniformity by strengthening inter-fiber collisions and breaking agglomerates. Optimized processing parameters (6-12 min mixing time and 600-1200 rpm mixing speed) effectively enhanced fluid shear and particle movement to homogenize CF distribution. However, excessively long stirring duration and excessive mixing speed generated parallel particle flow trajectories and suppressed valid inter-particle collisions. Specifically, a high mixing speed of 1400 rpm induced prominent fiber orientation and slight secondary re-agglomeration, thereby degrading the mixing quality. The multi-scale coupling analysis of macroscopic statistical data and microscopic flow field evolution clarified the intrinsic particle-scale dispersion mechanism of PDMS/CF composites.

***Keywords:*** *PDMS/CF composite; Homogeneous mixture; EDEM; Mixing speed; Mixing time*

## 1 Introduction

With the rapid miniaturization and high-power integration of modern electronic devices, efficient thermal dissipation has become a critical bottleneck restricting device stability and service life[1,2]. Benefiting from low density, good flexibility, superior corrosion resistance and facile processability, polymers have been widely applied in electronic packaging and industrial thermal management [3]. Nevertheless, the intrinsically low thermal conductivity [often $\leqslant$ 0.5 W/(mK)[1]] greatly limits their practical application in high-efficiency heat dissipation scenarios. Embedding thermal fillers into polymer matrices has become a mainstream and effective strategy to fabricate thermally conductive composites[4,5].

The thermal performance of polymer composites significantly depends on the integrity and continuity of filler networks, where uniform filler dispersion is an essential prerequisite. Duing blending processes, microscale fillers easily aggregate under van der Waals forces and electrostatic adsorption[6]. Severe filler agglomeration disrupts the continuity of filler network, and ultimately degrades the thermal performance of polymer composites. The dispersion quality is governed by the dynamic competition between inter-filler agglomeration forces and external flow shear force. Compared with the inherent filler agglomeration characteristics, the shear-induced dispersion effect can be effectively tailored by optimizing mixing techniques and processing parameters. As an advanced manufacturing method, planetary centrifugal mixing integrates chamber revolution and autorotation to generate complex flow gradients and strong centrifugal-shear coupling effects. This unique working principle effectively breaks filler agglomerates and improves filler uniformity, exhibiting distinct advantages over conventional stirring methods. Although this technique has been widely adopted to



Received: April 13, 2026; Accepted: May 25, 2026

prepare mixtures, most available studies only focus on the macroscopic relationship between processing parameters and thermal performance of mixtures. The microscale dynamic dispersion behavior of fillers during planetary centrifugal blending, as well as the underlying particle-level dispersion mechanism, remains insufficiently clarified, restricting the precise optimization of this blending process[7,8].

In this study, polydimethylsiloxane (PDMS) was selected as polymer matrix and carbon fiber (CF) served as thermal filler. Based on EDEM software[9], the dispersion evolution of fillers varying with filler content, mixing time and mixing speeds was studied. By correlating macroscopic mixing deviation statistics with microscopic particle flow field characteristics, this study aims to reveal the intrinsic dispersion mechanism of PDMS/CF composites, providing theoretical support and process guidance for the fabrication of polymer composites.

## 2 Simulation Experiments

### 2.1 Model construction

Planetary centrifugal vacuum mixers realize homogeneous mixture blending through the coupled revolution and autorotation of the mixing chamber. The dual rotational motions (revolution and autorotation) impose strong centrifugal loading to drive intense relative particle movement inside the cavity. A cylindrical mixing chamber with an inner diameter of 60 mm and axial length of 47 mm was established within the EDEM simulation framework [Figure 1(a)]. Identical clockwise rotational velocity was prescribed for both chamber revolution and autorotation. Particle dimensions were reasonably scaled to accelerate simulation computation: PDMS was represented by 0.55 mm spherical discrete elements, while CF was modeled as cylindrical particles with a 0.055 mm cross-sectional diameter and 6 mm fiber length. All particles were initialized via static generation, with a preset settling velocity of 1 mm/s. The particle injection rate was defined as 500 particles/s for PDMS spheres and 100 particles/s for CF cylinders. After bulk particle filling finished, the mixing simulation commenced, with gravitational acceleration (9.81 m/s$^2$) adopted as the sole external environmental field. Polyvinyl chloride (PVC) was assigned as the chamber wall structural material. Key intrinsic material parameters are summarized in Table 1. For contact mechanics assignment, the Johnson–Kendall–Roberts (JKR) adhesion model was applied for PDMS–CF inter-particle contacts, PDMS self-contacts, and PDMS–PVC wall interactions. The standard Hertz–Mindlin (no slip) contact model was deployed for CF inter-particle collisions and contact between CF segments and the chamber inner wall.

**Table 1** Material physical parameters adopted in EDEM simulations

| Materials | Density (kg/m$^3$) | Shear Modulus (Pa) | Poisson's Ratio |
|---|---|---|---|
| PDMS | 1030 | 1.715×106 | 0.49 |
| CF | 2200 | 6×1010 | 0.25 |
| PVC | 1450 | 3.501×109 | 0.30 |

### 2.2 Evaluation metric for particle mixing uniformity

Mixing deviation (σ) was adopted as the quantitative indicator to characterize filler dispersion quality. With the built-in meshing module embedded in EDEM, the mixing chamber computational domain was discretized uniformly along the X, Y and Z axes to generate a total of $n^3$ cubic voxels [Figures 1(b-d)]. After tallying the particle category and particle count confined within each individual voxel, the local mixing degree of every grid cell alongside the bulk-averaged mixing degree across all voxels can be acquired. σ is subsequently solved via Equation :

$$\sigma = \sqrt{\frac{\sum_{i=1}^{n^3}\left(M_i - \bar{M}\right)^2}{n^3}}$$

where $M_i$ denotes the mixing degree of the *i*-th voxel, and $\bar{M}$ is the average mixing degrees of all voxels.

Referring to the grid layout visualized in Figures 1(b)–(d), the mixing vessel is split into 343 discrete voxels (7 partitions along each coordinate axis). Grid cells holding under 20 particles are eliminated from subsequent statistical calculation, which mitigates measurement noise stemming from inadequate particle sampling and suppresses unnecessary computational bias.

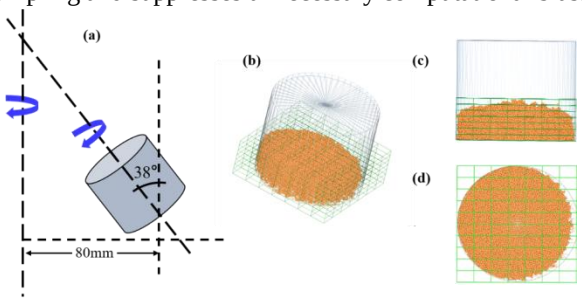


**Figures 1** (a) Schematic diagram of the mixing chamber; (b-d) Grid division diagrams.

## 3 Results and Discussion

### 3.1 Effect of filler content

Figure 2 shows the effect of CF contents on the mixing deviation. Obviously, mixing deviation shows a clear monotonic reduction as CF loading increases under identical stirring operating conditions. A peak value of 0.56 was obtained at 1 vol% CF. Progressive declines in mixing deviation were recorded with the increasing of filler loading, with approximate values of 0.55, 0.53, 0.49 and 0.478 for CF of 2, 3, 4 and 5 vol%, respectively. Such a downward tendency stems from amplified inter-filler collision behaviors at higher CF loading level during planetary centrifugal blending. Greater contact frequency between individual CFs breaks filler agglomerates subjected to centrifugal shear stress, restraining cluster regeneration and improving bulk dispersion performance. The results indicate that raising CF content within the 1-5 vol% range promotes the uniform dispersion of filler, which provides desirable microstructural prerequisites to construct interconnected filler networks in the samples.

### 3.2 Effect of mixing time and mixing speed

As for the mixing time [Figure 3(a)], mixing deviation decreases sharply from 6 to 12 min, after which the curve plateaus with negligible variation at 14 min; this indicates that prolonged stirring beyond the equilibrium durations brings negligible improvement in filler dispersion. Figure 3(b) shows the variation of mixing deviation under different mixing speeds. It is obvious that mixing deviation decreases persistently with the mixing speed increase from 600 to 1200 rpm, indicating more uniform filler distribution. However, 1400 rpm triggers a slight growth of deviation, meaning excessive mixing speed weakens filler dispersion quality.

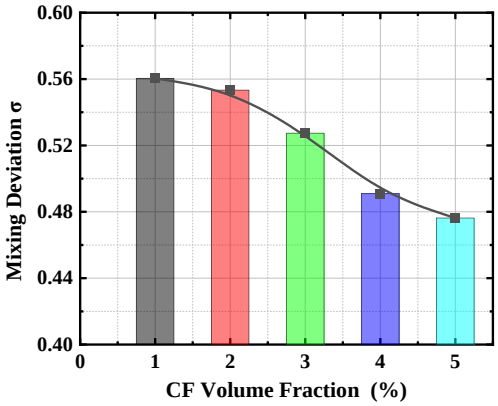


**Figure 2** Mixing deviation varying with CF loading level

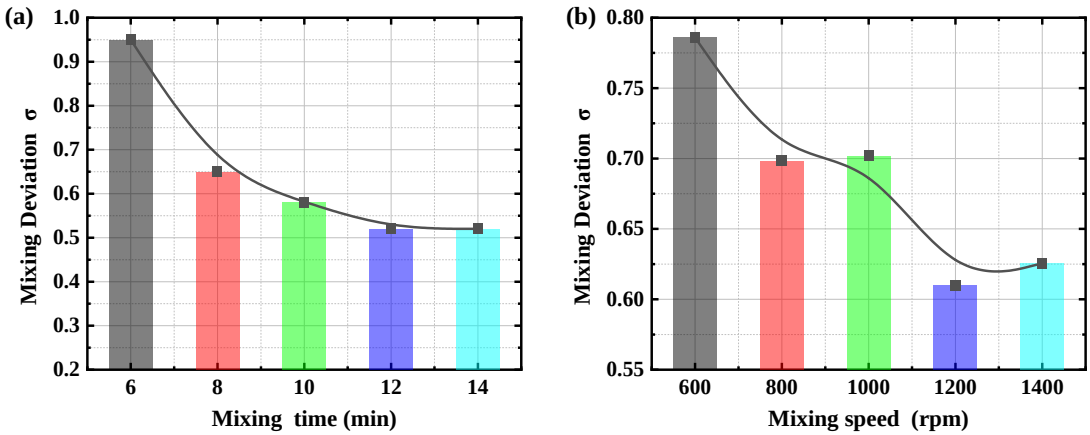


**Figure 3** Evolutions of mixing deviation varying with: (a) mixing time, and (b) mixing speed

The microscale particle kinematic features captured by velocity nephograms (Figure 4 and 5) elaborate the underlying physical mechanisms governing the above macroscopic pheonomenon (Figure 3). As for mixing-time (Figure 4), at the mixing duration of 6 min, distinct discrepancies exist in the flow orientations of particles. The resulting relative velocity drives frequent inter-particle collisions, which continuously break CF agglomerates under shear loading and improve filler dispersion, corresponding to the sharp decline of macroscopic mixing deviation. When mixing lasts for 12 min, the flow trajectories of most particles become nearly parallel with negligible relative velocity, bringing inter-particle collisions to a near halt so that the dispersion enhancement relying on collision-induced cluster fracture no longer works. Further extending the mixing duration to 14 min produces no noticeable shifts in particle velocity magnitude and flow orientation, as the spatial arrangement of fillers reaches dynamic equilibrium. Extra stirring time fails to further upgrade dispersion homogeneity, which explains the stable plateau segment observed on the mixing deviation curve with negligible process optimization benefits.

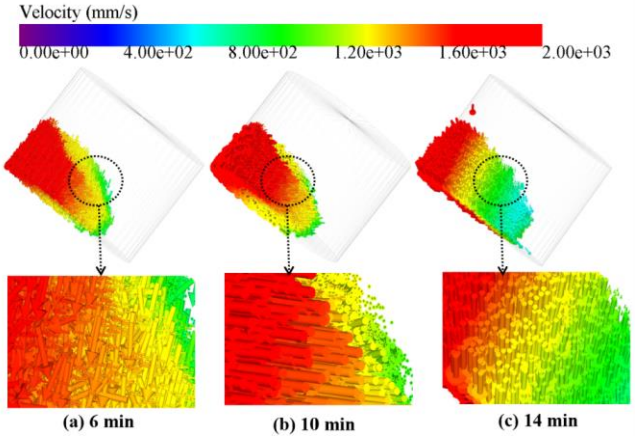


**Figure 4** Particle velocity contour distributions at mixing time of: (a) 6 min; (b) 10 min; (c) 14 min

For the mixing speed (Figure 5), as mixing speeds below 1000 rpm, prominent differences in particle flow directions create considerable relative velocity, triggering frequent inter-filler collisions during mixing. Sustained collision and shear effects continuously disintegrate filler agglomerates, thus steadily improving CF homogeneity and reducing mixing deviation. When the mixing speed rises to 1400 rpm, nearly parallel particle flow trajectories are observed with negligible relative velocity, which greatly suppresses inter-particle collisions and invalidates the cluster-breaking mechanism dominated by particle impact. Further increasing the mixing speed cannot promote the uniformity of filler spatial distribution; severe fiber orientation induced by excessive centrifugal force even may cause slight secondary re-agglomeration, leading to a mild rebound of macroscopic mixing deviation.

Combined the results of mixing deviation statistics and particle flow fields demonstrates that moderate mixing time and mixing speed facilitate uniform filler dispersion. Excessively harsh mixing parameters weaken dispersion performance; the revealed particle-level mechanisms provide guidance for optimizing the preparation process of PDMS/CF composites.

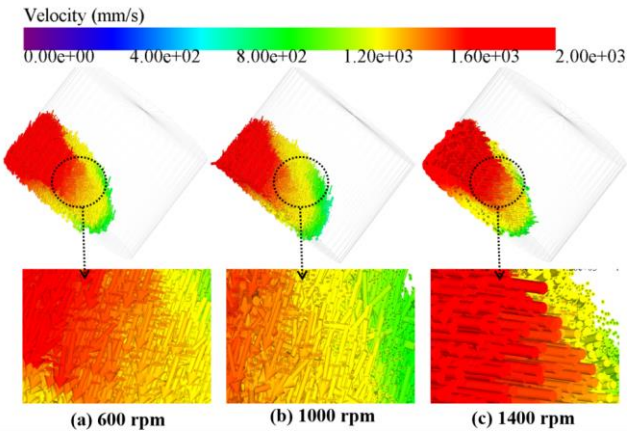


**Figure 5** Particle velocity contour distributions varying with mixing speed: (a) 600 rpm; (b) 1000 rpm; (c) 1400 rpm

## 4 Conclusions

In this study, discrete element simulations based on the EDEM software were performed to investigate the dispersion behavior of CFs within PDMS matrix by planetary centrifugal blending, where mixing deviation was adopted as the quantitative index to evaluate filler homogeneity. The effect of three parameters (namely CF fraction, mixing time and mixing speed) on the the dispersion quality of PDMS/CF composites were studied. Within CF loading level of 1-5 vol%, elevated filler concentration effectively reduced mixing deviation and promoted uniform CF distribution, which was attributed to intensified inter-filler collisions that disintegrate fiber agglomerates. Enhancing mixing time from 6 to 10 min, and mixing speed from 600 to 1000 rpm also facilitated filler homogenization via enhancing fluid shear and particle contact frequency. However, obvious performance plateaus emerged once mixing time exceeded 12 min and mixing speed surpassed 1200 rpm; further increasing either parameter generated negligible improvements in dispersion uniformity, while a mixing

speed of 1400 rpm even degraded mixing performance. These findings deliver clear theoretical guidance and process optimization references for the fabrication of polymer composites via planetary centrifugal blending, and offer generalizable insights for the formulation design of other polymer composites.

**Funding:** Projects (2021JJ40536) supported by the Natural Science Foundation of Hunan Province.

## References

[1] He, X., Li, Q., Li, L., et al. Preparation of a flexible polymer-based phase change composite with enhanced thermal management enabled by low-heat-dissipation structure [J]. Thermal Science and Engineering Progress, 2026, 69: 104433.

[2] Wu, J., Yang, T., Wang, K., et al. Revealing the role of molecular weight on mechanical reinforcement of highly oriented UHMW-PE fibers [J]. Polymer, 2025, 317: 127953.

[3] He, L., Dou, Z., Zhang, Y., et al. Modelling Effective Thermal Conductivity in Polymer Composites: A Simple Cubic Structure Approach [J]. Composites Science and Technology, 2020, 184: 107775.

[4] Zheng, S., Wang, Y., Guo, L., et al. Research progress of thermally conductive polymer composites with three-dimensional interconnected network structures [J]. Acta Materiae Compositae Sinica, 2023, 40(12): 6528-6544.

[5] Tang, S., Liu, S. L., Cong, B. H., et al. Graph attention networks decode conductive network mechanism and accelerate design of polymer nanocomposites [J]. NPJ Computational Materials, 2025, 11: 280.

[6] Cheremisinoff, Nicholas P. Polymer mixing and extrusion technology [M]. N. Y.: Dekker, 1987.

[7] Kwon Joong Son. Numerical analysis of viscous polymer resin mixing processes in high-speed blade-free planetary blender using smoothed particle hydrodynamics[J]. Processes, 2023, 11(9): 2555.

[8] Xin, Y., Zhu, X., Wang, T.. Mixing characteristics of polymer melt in triple screw extruders with combined screws using finite element method[J]. IOP Conference Series: Materials Science and Engineering, 2020, 768(2): 022068.

[9] Graziano Frungieri, Gianluca Boccardo, Antonio Buffo, et al. CFD-DEM characterization and population balance modelling of a dispersive mixing process[J]. Chemical Engineering Science, 2022, 260: 117859.

Viser Technology Pte. Ltd.
Research and Application of Materials Science
DOI: 10.33142/rams.v8i1.20146

Research Article Open Access

# Preparation and Performance Regulation of Carbon-Fiber-Reinforced PC/ABS Composites for Microwave Absorption and EMI Shielding

**WenTao YU[1,2], Jichao DING[3], Liting HAO[3], Lulin WANG[1*], Yeming XIAN[1*]**

1. Guangzhou Super-Dragon Engineering Plastics Co.Ltd, Guangzhou, 510440, China

2. College of New Materials and Chemical Engineering, Beijing Institute of Petrochemical Technology, Beijing, 102617, China

3. School of Chemical Engineering, Dalian University of Technology, Dalian, Liaoning, 116024, China

*Corresponding Author: Lulin WANG, E-mail: hulin@gzselon.com; Yeming Xian, E-mail: xianyeming@gzselon.com

**Abstract**

The rapid development of high-frequency electronic devices and fifth-generation wireless communication systems has increased the demand for polymer-based materials with both electromagnetic interference shielding and microwave absorption capabilities. In this work, carbon-fiber-reinforced polycarbonate/acrylonitrile–butadiene–styrene composites were prepared by twin-screw melt compounding, and the effects of carbon fiber content, fiber type, and feeding strategy on the mechanical and electromagnetic properties were investigated. Two feeding modes, namely main feeding and side feeding, were compared to regulate the fiber length distribution and conductive-network structure in the PC/ABS matrix. Compared with main feeding, side feeding effectively reduced fiber breakage during extrusion. For example, the number-average fiber length of MC10%-SF reached 165.7 μm, whereas that of MC10% prepared by main feeding was only 111.7 μm. The retained long fibers promoted the formation of continuous conductive pathways, leading to enhanced dielectric loss and improved electromagnetic attenuation. Among the investigated formulations, MC20%-SF exhibited a maximum reflection loss of -51 dB at 15.5 GHz with a thickness of 1.7 mm and an effective absorption bandwidth of 4.56 GHz. Meanwhile, it maintained favorable mechanical properties, including a tensile strength of 115 MPa and a flexural modulus of 13,249 MPa. For EMI shielding, HC30%-SF achieved a total shielding effectiveness close to 55 dB in the X-band. These results indicate that controlling fiber length through side feeding is an effective strategy for balancing mechanical reinforcement, microwave absorption, and EMI shielding performance in PC/ABS-based conductive composites.

*Keywords:* *PC/ABS composites; carbon fiber; side feeding; fiber length distribution; microwave absorption; EMI shielding*

## 1 Introduction

The rapid deployment of fifth-generation wireless communication systems, automotive radar, and high-frequency electronic devices has intensified electromagnetic interference problems in confined electronic environments. Electromagnetic interference not only deteriorates signal transmission quality but may also affect the reliability and safety of electronic components[1]. Therefore, lightweight polymer-based materials capable of electromagnetic interference shielding and microwave absorption have attracted increasing attention. Compared with traditional metallic shielding materials, conductive polymer composites offer advantages such as lower density, easier processing, corrosion resistance, and greater design flexibility.

Polycarbonate (PC) is one of the most widely used engineering thermoplastics owing to its high impact resistance, dimensional stability, heat resistance, and good processability[2]. PC/ABS blends further combine the toughness of PC with the improved melt processability of ABS, making them suitable for housings and structural components in electronic and



Received: April 15, 2026; Accepted: May 29, 2026

automotive applications. However, both PC and PC/ABS are electrically insulating and exhibit limited electromagnetic wave attenuation. Introducing conductive fillers into PC/ABS matrices is therefore an effective route to impart electromagnetic functionality while retaining the advantages of thermoplastic processing.

Carbon fibers are promising conductive fillers because of their high aspect ratio, electrical conductivity, thermal stability, and mechanical reinforcement capability. When dispersed in a polymer matrix, carbon fibers can form interconnected conductive networks, which contribute to conduction loss, interfacial polarization, and multiple reflection of electromagnetic waves[3-4]. However, the final electromagnetic performance of carbon-fiber-reinforced polymer composites is strongly influenced by the fiber length, dispersion state, and interfacial morphology. During melt compounding, excessive shear may cause severe fiber breakage, reducing the effective aspect ratio and increasing the percolation threshold. As a result, the construction of an efficient conductive network in PC/ABS composites remains challenging.

In this study, carbon-fiber-reinforced PC/ABS composites were prepared by twin-screw extrusion. The effects of carbon fiber content and feeding strategy were systematically investigated. In particular, main feeding and side feeding were compared to clarify the role of fiber length retention in determining mechanical properties, dielectric response, microwave absorption, and EMI shielding effectiveness. The relationship among processing, microstructure, and electromagnetic performance was analyzed to provide a practical strategy for preparing multifunctional PC/ABS composites for high-frequency electronic applications.

## 2 Experimental

### 2.1 Materials

Polycarbonate resin was supplied by Mitsubishi Engineering-Plastics Corporation. Acrylonitrile–butadiene–styrene resin was obtained from LG Chem. Two commercial carbon fibers, CFUW-MC C-6 and CFEPU-HC C-6, supplied by Toray Industries, were used and denoted as MC and HC, respectively. Carbon black was used as a secondary conductive filler. Irganox 168 and Irganox 1076 were used as antioxidants. A methyl methacrylate–butadiene–styrene copolymer was employed as the toughening agent, and pentaerythritol tetrastearate was used as the lubricant. All materials were dried according to standard processing requirements before extrusion.

### 2.2 Composite preparation

PC/ABS/CF composites were prepared by melt compounding using a co-rotating twin-screw extruder with a screw diameter of 35 mm and an L/D ratio of 40:1. The formulations are listed in Table 1. PC, ABS, carbon black, antioxidants, toughening agent, and lubricant were premixed in a high-speed mixer and introduced through the main hopper. For the main-feed samples, carbon fibers were also fed through the main hopper and therefore experienced the entire screw shear history. For the side-feed samples, carbon fibers were introduced through a downstream side feeder to reduce their residence time and shear exposure. The barrel temperature was set between 220 and 260 ℃ from the feeding zone to the die, and the screw speed was maintained at 300 rpm. The extrudates were water-cooled, pelletized, and dried at 120 ℃ for 4 h before injection molding and characterization.

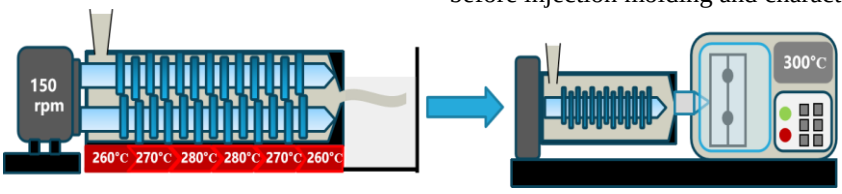


**Figure 1** Schematic diagram of preparation process flow of PC/ABS/CF composites

**Table 1** Formulations of PC/ABS/CF composites (wt%)

| Sample | PC | ABS | CF (MC) | CF (HC) | CB | Antioxidants | Toughener | Lubricant |
|---|---|---|---|---|---|---|---|---|
| PC/ABS | 65.8 | 28.2 | — | — | 2.5 | 0.3 | 3.0 | 0.2 |
| MC10% | 58.8 | 25.2 | 10 | — | 2.5 | 0.3 | 3.0 | 0.2 |
| MC20% | 51.8 | 22.2 | 20 | — | 2.5 | 0.3 | 3.0 | 0.2 |
| MC30% | 44.8 | 19.2 | 30 | — | 2.5 | 0.3 | 3.0 | 0.2 |
| HC10% | 58.8 | 25.2 | — | 10 | 2.5 | 0.3 | 3.0 | 0.2 |
| HC20% | 51.8 | 22.2 | — | 20 | 2.5 | 0.3 | 3.0 | 0.2 |
| HC30% | 44.8 | 19.2 | — | 30 | 2.5 | 0.3 | 3.0 | 0.2 |

## 3 Characterization

### 3.1 Mechanical properties

The PC/ABS/CF composites undergo preparation via melt compounding using a co-rotating twin-screw extruder (screw diameter: 35 mm, L/D ratio: 40:1). The formulations appear in Table 1. PC, ABS, carbon black, antioxidants, a toughening agent, and a lubricant mix in a high-speed mixer and feed through the main hopper. In the main-feed series, carbon fibers also enter through the main hopper alongside the other components, exposing the fibers to the full screw shear history. In the side-feed series, carbon fibers are introduced separately through a side-feed. The mechanical properties of the PC/ABS/CF composites are summarized in Table 2. With the increase in the amount of carbon fiber added, the rigidity of the material increases while its toughness decreases, manifested as an increase in strength modulus and a decrease in elongation. When carbon fiber is added through side feeding and the content is below 30%, the mechanical properties of the material exhibit the same trend. However, when the content reaches 30%, the mechanical properties decline, which is caused by poor compatibility between the matrix and carbon fiber.

### 3.2 Morphology and fiber length distribution

The fracture surfaces of the composites after cryogenic fracture were examined by scanning electron microscopy. Before observation, the specimens were sputter-coated with a thin layer of gold to reduce charging. For fiber length analysis, the polymer matrix was removed by dissolution in dichloromethane, and the extracted fibers were collected, dispersed on glass slides, measured from optical microscopy images and used self-developed software to count and calculate the length[5]. At least 300 fibers were counted for each sample to obtain representative length distributions.

We extracted fibers from the composites and measured their length distributions (Table 3). For MC10%, main-feeding gave a number, average length of 111.7 μm; side-feeding raised it to 165.7 μm. The improvement persisted at 20 wt% (106.0→146.4 μm) and 30 wt% (97.2→134.9 μm). Weight-average and cubic-average lengths followed the same trend. In both feeding modes, increasing fiber content reduced average length, which we link to higher melt viscosity and more frequent fiber-fiber collisions that cause breakage. But the distribution width remained narrow (1.20-1.30), indicating that side-feeding shifts the whole distribution toward longer values rather than creating a bimodal population. SEM images (Figure 2) visually confirm this: Longer retained fibers provide a higher effective aspect ratio, improve the continuity of the reinforcing network, and enhance load transfer within the PC/ABS matrix. This explains why the side-feed composites exhibited better tensile and flexural properties than the main-feed composites at the same carbon fiber content.

**Table 2** Mechanical properties of PC/ABS/CF composites.

| | Tensile strength / MPa | Elongation at break/ % | Impact strength / kJ ㎡ ⁻ ² | Flexural strength / MPa | Flexural modulus / MPa |
|---|---|---|---|---|---|
| Pure PC/ABS | 54 | 29.7 | 43.4 | 86.6 | 2442 |
| MC 10% | 64.9 | 5.3 | 5.79 | 102.7 | 4538 |
| MC 20% | 72.1 | 4.2 | 4.39 | 113 | 6736 |
| MC 30% | 96.4 | 3.85 | 4.12 | 144 | 11742 |
| HC 10% | 60.8 | 6.1 | 5.59 | 97.1 | 3987 |
| HC 20% | 68.5 | 4.8 | 4.08 | 123 | 9668 |
| HC 30% | 81.3 | 3.6 | 3.46 | 110 | 6567 |
| MC 10%-SF | 95.4 | 3.8 | 7.14 | 137.4 | 7731 |
| MC 20%-SF | 115 | 3.6 | 6.59 | 173.8 | 13249 |
| MC 30%-SF | 114 | 3.7 | 6.88 | 162.3 | 10756 |
| HC 10%-SF | 84.5 | 3.9 | 6.87 | 143 | 8297 |
| HC 20%-SF | 109 | 3.3 | 5.92 | 176 | 13781 |
| HC 30%-SF | 114 | 3.6 | 6.33 | 166.2 | 10751 |

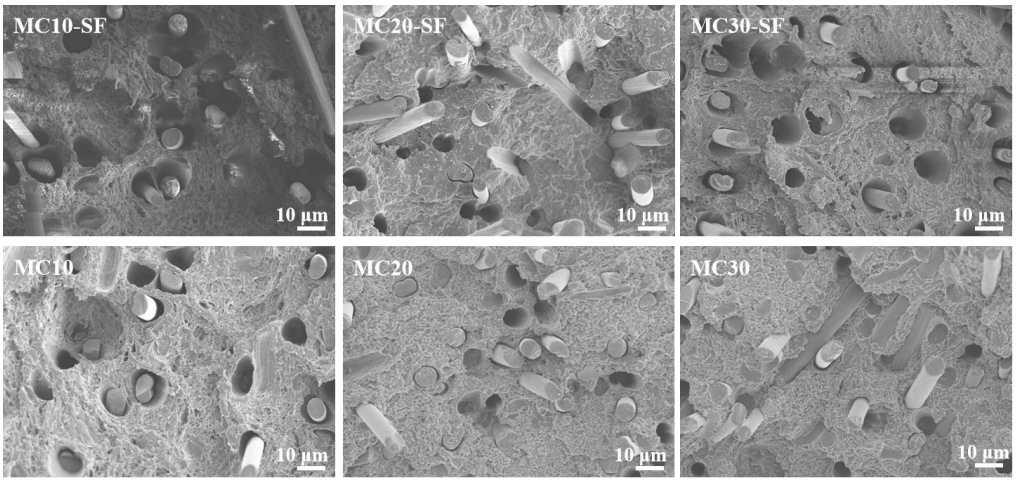


**Figure 2** The SEM image of PC/ABS/CF composites

**Table 3** Fiber length distribution parameters of carbon fibers extracted from composites.

| | Number-average Length/μm | Weight-average Length/μm | Mean Cubic Length/μm | Distribution Width |
|---|---|---|---|---|
| MC10%-SF | 165.67 | 206.3 | 247.27 | 1.25 |
| MC20%-SF | 146.37 | 175.67 | 204.92 | 1.2 |
| MC30%-SF | 134.94 | 175.27 | 215.24 | 1.3 |
| MC10% | 111.72 | 134.84 | 161.23 | 1.21 |
| MC20% | 106.02 | 135.28 | 177.45 | 1.28 |
| MC30% | 97.21 | 116.49 | 140.83 | 1.2 |

### 3.3 Dielectric properties

The complex permittivity of the composites was measured in the frequency range of 2-18 GHz using a vector network analyzer and the coaxial transmission-line method. The specimens were machined into circular ring samples with an outer diameter of 7.0 mm, an inner diameter of 3.0 mm, and a thickness of 2.0-3.0 mm.

The complex permittivity (ε′ and ε″) of the composites in the 2-18 GHz range appears in Figure 3. Because no magnetic components are included in the formulations, the complex permeability (μ′ and μ″) remains approximately 1.00 and 0.00, respectively, throughout the entire frequency range. Consequently, the electromagnetic wave attenuation of these composites is primarily determined by dielectric loss rather than magnetic loss.

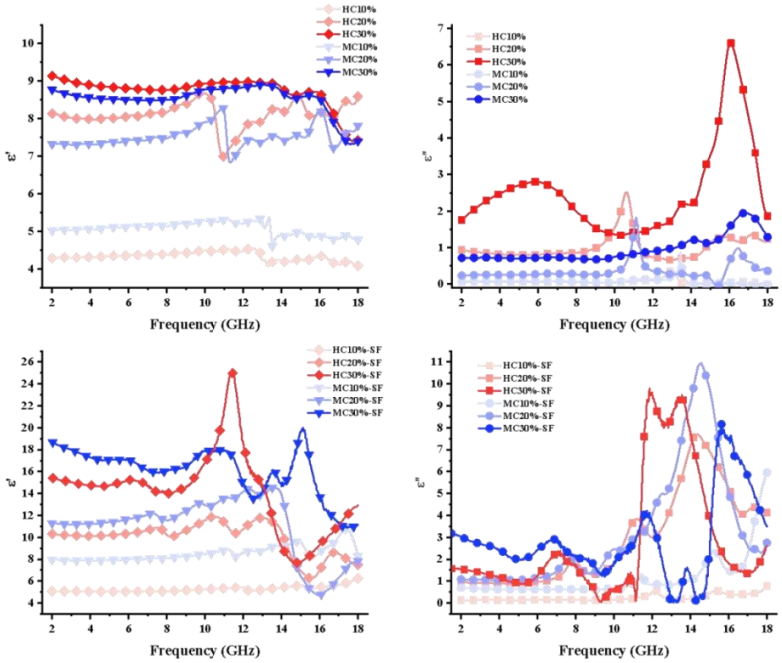


**Figure 3** The complex permittivity of PC/ABS/CF composites

Both the real (ε′) and imaginary (ε″) parts of the permittivity increased with increasing CF content, consistent with the enhanced polarization and conductive loss contributions from the carbon fibers. The side-feed series exhibited significantly higher permittivity values than the main-feed series at equivalent CF loading. For example, at 10 GHz, ε′ for MC20%-SF reached approximately 25, compared to ~15 for MC20% (main-feed). This enhancement is attributed to the longer fibers in the side-feed composites, which more readily form conductive pathways and facilitate charge transport within the matrix.

### 3.4 EMI Shielding effectiveness

The scattering parameters ($S_{11}$ and $S_{12}$) of the composites were measured using the waveguide method over the X-band frequency range (8.0-12.6 GHz). The EMI shielding effectiveness (SE), including total shielding effectiveness ($SE_T$), absorption ($SE_A$), and reflection ($SE_T$), was calculated from the scattering parameters according to the following equations[6]:

$$R = |S_{11}|^2,\ T = |S_{21}|^2,\ A = 1 - R - T \quad (1)$$

$$SE_T = SE_R + SE_A + SE_M \quad (2)$$

$$SE_R = -10\log_{10}(1 - R) \quad (3)$$

$$SE_A = -10\log_{10}\left[\frac{T}{1 - R}\right] \quad (4)$$

The EMI shielding effectiveness of the composites was evaluated in the X-band, and the results are shown in Figure 5. The total shielding effectiveness increased with increasing carbon fiber content for both the main-feed and side-feed series. At the same filler loading, the side-feed composites exhibited higher shielding effectiveness than the main-feed composites, which can be attributed to the more continuous conductive networks formed by the longer retained fibers.

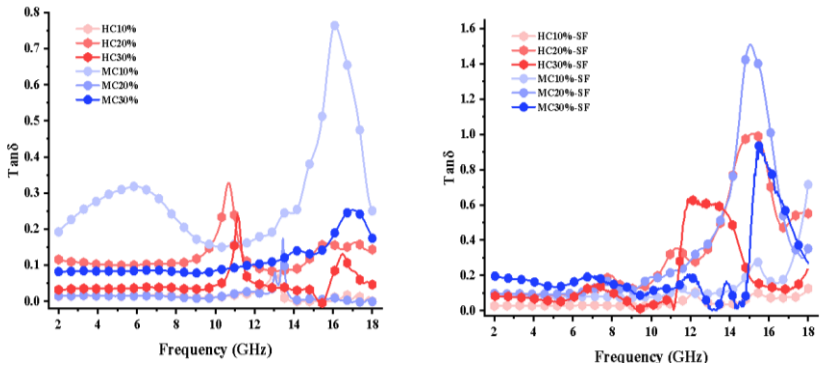


**Figure 4** The dielectric loss tangent of PC/ABS/CF composites

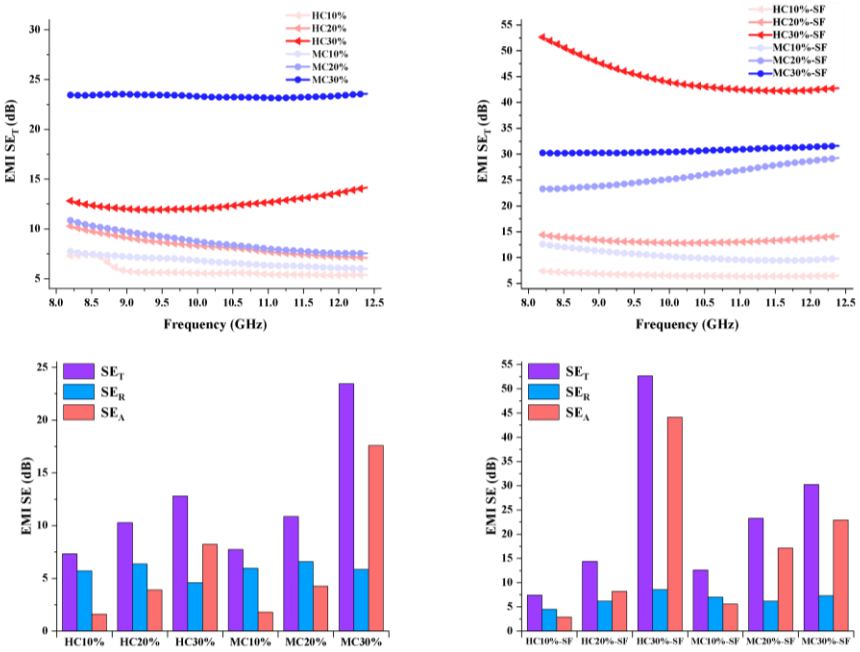


**Figure 5** The shielding effectiveness of PC/ABS/CF composites

Among all samples, HC30%-SF achieved a total shielding effectiveness close to 55 dB at 10 GHz. This value is sufficient for many practical EMI shielding applications. The enhanced shielding performance originates from the combined effects of reflection and absorption. At low carbon fiber loading, reflection contributes significantly to the total shielding because of the impedance mismatch between air and the conductive composite surface. As the carbon fiber content increases, the conductive network becomes denser, and absorption gradually becomes the dominant shielding mechanism. The increased absorption contribution is related to ohmic loss, interfacial polarization, and multiple scattering within the interconnected fiber network.

The transition from reflection-dominated shielding to absorption-dominated shielding is beneficial for electromagnetic compatibility applications because absorption can reduce secondary electromagnetic pollution caused by reflected waves. Therefore, side feeding not only improves the magnitude of shielding effectiveness but also promotes a more favorable shielding mechanism.

### 3.5 Microwave absorption performance

The reflection loss (RL) of the composites was calculated from the measured electromagnetic parameters using the transmission-line theory. For a single-layer absorber backed by a perfect conductor, the input impedance ($Z_{in}$) at the absorber surface is given by the following equations[7]:

$$Z_{in}=Z_0\sqrt{\mu_r\varepsilon_r}\tanh\left[j\left(\frac{2\pi fd}{c}\right)\sqrt{\frac{\mu_r}{\varepsilon_r}}\right] \quad (5)$$

$$RL=20lg\left|\frac{Z_{in}-Z_0}{Z_{in}+Z_0}\right| \quad (6)$$

where f is the frequency, d is the absorber thickness, c is the speed of light, and $Z_0$ is the impedance of free space (377 Ω). The RL values were calculated for absorber thicknesses ranging from 1.0 to 5.5 mm to identify the optimal thickness for maximum absorption at each frequency.

The microwave absorption performance of the composites was evaluated by calculating the reflection loss based on transmission-line theory. The maximum reflection loss, corresponding matching thickness, matching frequency, and effective absorption bandwidth are summarized in Table 4. The neat PC/ABS blend exhibited negligible microwave absorption, with a reflection loss of approximately -2 dB, confirming that the polymer matrix itself has limited electromagnetic attenuation capability.

As shown in the Table 4, the addition amount and dispersion length of $SE_T$ are directly proportional to the amount of carbon fiber added. For the side-feeding series, HC30% $SE_T$ can reach nearly 55 dB. According to the SE distribution diagram of the sample at a frequency of 8.0 GHz, when the carbon fiber content is between 10% and 20%, SE is mainly contributed by $SE_R$ ($SE_R > SE_A$), indicating that the electromagnetic shielding of the sample is achieved through both electromagnetic wave reflection and absorption, with a higher proportion of reflection. When the content is at 30%, SE is mainly contributed by $SE_A$, and electromagnetic shielding is mainly achieved through electromagnetic wave absorption. The same trend is even more pronounced in the side-feeding system. When the addition reaches 20%, $SE_A$ has already begun to exceed $SE_R$, indicating that when carbon fibers form a conductive network in the matrix, they can absorb electromagnetic waves through conductivity loss, thus achieving better electromagnetic shielding performance. Therefore, the electromagnetic wave absorption (wave absorption) of the sample and the influence of carbon fiber distribution and dispersion length on the material's wave absorption behavior must be explored in detail.

**Table 4** Microwave absorption properties of PC/ABS/CF composites.

| | Maximum Reflection Loss/dB | Effective Absorption Bandwidth/ GHz |
|---|---|---|
| Pure PC/ABS | -2 | - |
| MC 10%-SF | -40 (4.7 mm,17.0 GHz) | 1.76 |
| MC 20%-SF | -51 (1.7 mm,15.5 GHz) | 4.56 |
| MC 30%-SF | -45 (4.6 mm,14.2GHz) | 4.80 |
| HC 10%-SF | -11 (5.3 mm,18.0 GHz) | - |
| HC 20%-SF | -52 (1.6 mm,15.8 GHz) | 3.68 |
| HC 30%-SF | -39 (1.6 mm,11.2 GHz) | 2.80 |
| MC 10% | -5.7 | - |
| MC 20% | -15 (5.2 mm,16.4 GHz) | 0.96 |
| MC 30% | -54 (2.4 mm,7.7 GHz) | 4.80 |
| HC 10% | -5.57 | - |
| HC 20% | -21 (5.4 mm,15.6 GHz) | 1.60 |
| HC 30% | -46 (2.7 mm,7.2 GHz) | 4.64 |

Therefore, the improved absorption performance of MC20%-SF and HC20%-SF can be attributed to a better balance between impedance matching and attenuation capability. The results demonstrate that side feeding is an effective processing strategy for preparing PC/ABS/CF composites with both good microwave absorption and EMI shielding properties.

## 4 Conclusion

In this work, carbon-fiber-reinforced PC/ABS composites were prepared by twin-screw melt compounding, and the influence of feeding strategy on fiber length retention, mechanical properties, dielectric behavior, microwave absorption, and EMI shielding performance was investigated. Compared with main feeding, side feeding effectively reduced fiber breakage during extrusion and preserved longer carbon fibers in the PC/ABS matrix. The number-average fiber length of MC10%-SF reached 165.7 μm, which was much higher than that of the corresponding main-feed sample.

The retained long fibers enhanced the formation of conductive networks and improved both mechanical reinforcement and electromagnetic attenuation. MC20%-SF exhibited a tensile strength of 115 MPa and a flexural modulus of 13,249 MPa, showing a significant improvement over the main-feed counterpart. In terms of microwave absorption, MC20%-SF achieved a maximum reflection loss of -51 dB at 15.5 GHz with a thickness of 1.7 mm and an effective absorption bandwidth of 4.56 GHz. For EMI shielding, HC30%-SF showed a total shielding effectiveness close to 55 dB in the X-band.

The results demonstrate that the feeding strategy is a key processing parameter for regulating the fiber length distribution and conductive-network structure in PC/ABS/CF composites. Side feeding enables a favorable balance among mechanical strength, microwave absorption, and EMI shielding performance, making the prepared composites promising candidates for high-frequency electronic devices, 5G communication equipment, and automotive electromagnetic protection applications.

## References


[1] Chen Z, Xu C, Ma C, et al. Lightweight and flexible graphene foam composites for high-performance electromagnetic interference shielding [J]. Adv Mater, 2013(9): 1296-1300.

[2] Myung Geun Jang, Seung Chan Ryu, Kyu Jin Juhn, et al. Effects of carbon fiber modification with multiwall CNT on the electrical conductivity and EMI shielding effectiveness of polycarbonate/carbon fiber/CNT composites [J]. Journal of Applied Polymer Science, 2018(14):47302.

[3] In Chol Kim, Kee Hae Kwon, Woo Nyon Kim.Effects of hybrid fillers on the electrical conductivity, EMI shielding effectiveness, and flame retardancy of PBT and PolyASA composites with carbon fiber and MWCNT[J].Journal of Applied Polymer Science, 2019(44):48162.

[4] Abbasi H, Antunes M, Velasco J I. Recent advances in carbon-based polymer nanocomposites for electromagnetic interference shielding [J]. Prog Mater Sci, 2019(13): 319-373.

[5] Xian Yeming. Method, device, and medium for extracting fiber information of composite materials based on unsupervised learning: 202410550187.6 [P]. 2024-05-06.

[6] Wentao Yu, Jiahui Lin, Zhaozhang Zhao, et al.Polyimide-based porous carbon and cobalt nanoparticle composites as high-performance electromagnetic wave absorbers [J].RSC Advance, 2024(14): 9716-9724.

[7] Xiaowen Wang, Paul Smith, Zhe Qiang, et al. Fire-retardant, self-extinguishing multiblock poly (esterimide)s/graphene composites with segregated structure for electromagnetic interference shielding [J]. Composites Part A, 2022(19):107262.

Viser Technology Pte. Ltd.
Research and Application of Materials Science
DOI: 10.33142/rams.v8i1.20147

Research Article Open Access

# Direct $CO_2$ Capture by Carbide Slag: Moisture Regulation, Uptake Performance, and Reaction Kinetics

**Chao LIU, Chao YANG, Chao ZHU**

Xi'an University of Architecture and Technology, Xi'an, Shanxi, 710055 China

*Corresponding Author: Chao LIU, E-mail:chaoliu@xauat.edu.cn

**Abstract**

To evaluate the feasibility of carbide slag as a low-cost calcium-based solid waste for $CO_2$ mineral capture, direct carbonation experiments were carried out under different moisture contents. The effects of moisture content on $CO_2$ uptake, carbonation efficiency, phase composition, and morphology were investigated. Five moisture contents of 0%, 5%, 10%, 20%, and 30% were selected, and $CO_2$ was introduced at ambient temperature and pressure. The results show that the abundant $Ca(OH)_2$ in carbide slag can react with $CO_2$ to form $CaCO_3$, indicating that carbide slag has potential for direct mineral carbonation of $CO_2$. As the moisture content increased from 0% to 20%, the $CO_2$ uptake of carbide slag gradually increased. The best carbonation performance was obtained at 20% moisture content, where the $CO_2$ uptake reached 4.60 mol/kg after 120 min, corresponding to a $CO_2$ fixation amount of 0.2024 g/g and a carbonation efficiency of 36.8%. When the moisture content increased further to 30%, the $CO_2$ uptake decreased to 3.20 mol/kg. TG/DTG, XRD, and FTIR results indicate that $Ca(OH)_2$ was gradually converted into $CaCO_3$ during carbonation. An appropriate amount of moisture promoted $CaCO_3$ formation and deposition, whereas excessive moisture hindered $CO_2$ diffusion and reduced the carbonation efficiency. These results demonstrate that moisture regulation is an important factor for improving the efficiency of direct $CO_2$ capture by carbide slag and provide a reference for low-cost $CO_2$ mineralization using alkaline industrial solid wastes.

***Keywords:*** *carbide slag; $CO_2$ capture; direct carbonation; moisture content; uptake capacity; reaction kinetics*

## 1 Introduction

With the continuous increase in $CO_2$ emissions from industrial production, the development of low-cost and easily implemented $CO_2$ capture and fixation methods is of great significance. Mineral carbonation is a stable $CO_2$ fixation route, in which calcium- or magnesium-containing materials react with $CO_2$ to form carbonate products. Compared with conventional absorption and adsorption methods, mineral carbonation can directly fix $CO_2$ in solid products, and the subsequent treatment is relatively simple. Therefore, the use of active calcium components in industrial solid wastes for $CO_2$ mineralization has gradually become an important direction for the synergistic development of solid-waste utilization and carbon-emission reduction[1-4].

Carbide slag is an industrial by-product generated during acetylene production through calcium carbide hydrolysis. Its main component is usually $Ca(OH)_2$, with minor amounts of $CaCO_3$, CaO, $SiO_2$, $Al_2O_3$, $Fe_2O_3$, and MgO[1,5-7]. Owing to its strong alkalinity and high moisture content, long-term stockpiling of carbide slag may cause land occupation, dust emission, and alkaline leachate. At the same time, these chemical characteristics make carbide slag a reactive calcium reservoir. $Ca(OH)_2$ can combine with $CO_2$ to form $CaCO_3$, so carbonation can both immobilize $CO_2$ and lower the alkalinity of the residue, improving the possibility of subsequent reuse [6,8-14].

In direct carbonation, the role of water is particularly sensitive. A small amount of water can provide a liquid pathway for $CO_2$ dissolution, $Ca(OH)_2$ dissolution, and $Ca^{2+}$ transport, which accelerates



Received: March 1, 2026; Accepted: April 18, 2026

carbonate precipitation. If the water content is too high, however, a continuous or thick water layer may develop around particles and partly fill the voids between them. Under that condition, the gas path becomes longer and $CO_2$ diffusion to unreacted $Ca(OH)_2$ is restricted. The carbonation response of carbide slag is therefore expected to depend on the balance between liquid-phase reaction promotion and gas-phase mass-transfer limitation[8,12,15-17].

On this basis, the present study examined carbide slag with controlled moisture contents to clarify how water dosage affects direct $CO_2$ uptake and reaction progression. Samples were carbonated under identical ambient conditions, and the reaction products were characterized by TG/DTG, XRD, FTIR, and pH testing. The time-dependent uptake data were further used to compare initial reaction rates and final fixation capacities.[8,9,13,15,18]. This study aims to provide an experimental reference for the use of carbide slag in low-cost $CO_2$ capture.

## 2 Materials and Methods

### 2.1 Raw materials

The carbide slag used in this study was an industrial by-product generated during acetylene production from calcium carbide hydrolysis. The raw carbide slag was gray-white powder or slurry and showed strong alkalinity. To reduce the influence of the initial moisture content on the experimental results, the raw carbide slag was dried in an oven at 105 ℃ for 24 h before testing. It was then ground and sieved to obtain dry carbide slag powder with a particle size below 75 μm. The dried carbide slag was used as the base sample for subsequent moisture regulation and direct $CO_2$ carbonation experiments.

To determine the basic properties of carbide slag, X-ray diffraction was used to analyze its main mineral phases, and thermogravimetric analysis was used to identify the thermal decomposition characteristics of $Ca(OH)_2$ and $CaCO_3$. Scanning electron microscopy was used to observe the original particle morphology. In addition, the pH of the leachate of raw carbide slag was measured to evaluate its initial alkalinity. These tests were used to determine the existing forms of active calcium components in carbide slag and to provide a basis for the analysis of subsequent $CO_2$ carbonation reactions [5,13,18].

### 2.2 Preparation of carbide slag samples with different moisture contents

To investigate the effect of moisture content on the direct carbonation performance of carbide slag for $CO_2$ capture, five moisture levels of 0%, 5%, 10%, 20%, and 30% were set based on the dry mass of carbide slag. The moisture content was defined as the ratio of the added water mass to the dry carbide slag mass. Specifically, a certain mass of dried carbide slag was weighed for each group, and the corresponding amount of deionized water was added according to the designed moisture content. After thorough mixing, the samples were sealed and stored for 24 h to allow relatively uniform moisture distribution.

The moisture content was calculated as follows:

$$w = \frac{m_w}{m_s} \times 100\% \quad (1)$$

Where w is the designed moisture content, $m_w$ is the mass of added water, and $m_s$ is the dry mass of carbide slag. No additional water was added to the 0% moisture sample, which represented the dry carbonation condition. The other groups represented carbide slag carbonation systems with different moisture contents. Through this grouping, $CO_2$ uptake under dry, low-moisture, medium-moisture, and relatively high-moisture conditions could be compared.

### 2.3 Direct $CO_2$ carbonation experiment

The direct $CO_2$ carbonation experiment was conducted at ambient temperature and pressure. The same mass of carbide slag samples with different moisture contents was uniformly spread in the reaction vessel to maintain an approximately consistent sample layer thickness. $CO_2$ gas was then continuously introduced into the reactor to ensure sufficient contact between the gas and the carbide slag sample and to initiate the carbonation reaction. To ensure comparability among different groups, the sample mass, gas flow rate, reaction temperature, reaction time, and sample spreading method were kept consistent during the experiments[8,9,13,15].

To obtain the variation of $CO_2$ uptake with reaction time under different moisture contents, four reaction times of 10, 30, 60, and 120 min were set. At each designated reaction time, the sample was removed and immediately sealed to reduce possible errors caused by further reaction with $CO_2$ or moisture in air. Each experiment was repeated at least three times, and the

average value was used for analysis.

The purpose of this experimental design was to compare the effect of moisture content on the direct carbonation efficiency of carbide slag. The 0% moisture group was used to characterize the $CO_2$ capture capacity under dry conditions; the 5% and 10% moisture groups were used to analyze the promoting effect of a small amount of water; the 20% moisture group was used to examine the reaction performance under medium moisture conditions; and the 30% moisture group was used to determine whether excessive moisture would inhibit $CO_2$ diffusion and carbonation. The experimental workflow is shown in Figure 1.

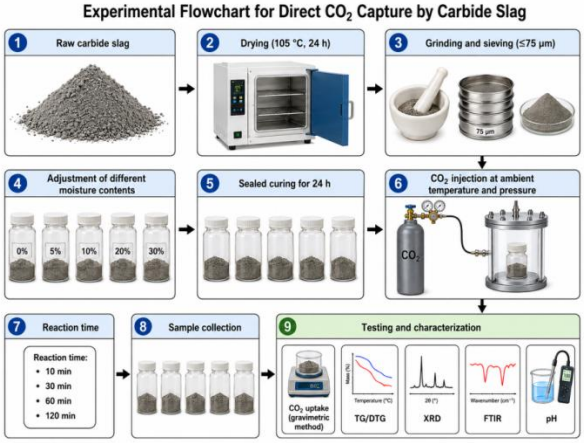


**Figure 1** Experimental flowchart for $CO_2$ capture by direct carbonation of carbide slag

### 2.4 Testing and characterization methods

X-ray diffraction was used to analyze the phase changes of carbide slag samples before and after carbonation, with particular attention to the characteristic peaks of $Ca(OH)_2$ and $CaCO_3$. By comparing the XRD patterns of samples carbonated under different moisture contents, the effect of moisture content on $Ca(OH)_2$ consumption and $CaCO_3$ formation could be evaluated[5,13,18].

Thermogravimetric analysis was used to measure mass loss during heating. Combined with DTG curves, the characteristic temperature ranges corresponding to $Ca(OH)_2$ dehydration and $CaCO_3$ decomposition with $CO_2$ release were identified. The $CO_2$ fixation amount and carbonation efficiency of carbide slag were calculated from the variation in $CaCO_3$ content before and after carbonation. Compared with the direct weighing method, the thermogravimetric method can reduce the influence of adsorbed water and free water on the calculation of $CO_2$ fixation amount[5,13,18].

Fourier transform infrared spectroscopy was used to analyze functional group changes in the carbonation products, with a focus on the characteristic absorption peaks of carbonate ions to further confirm $CaCO_3$ formation. pH tests were conducted to analyze the change in alkalinity before and after carbonation and to evaluate the alkalinity reduction effect of $CO_2$ carbonation on carbide slag[6,18,19].

### 2.5 Calculation of $CO_2$ fixation amount and carbonation efficiency

In this study, the $CO_2$ fixation amount during carbide slag carbonation was calculated using thermogravimetric results. $CaCO_3$ in the sample decomposes and releases $CO_2$ in the high-temperature range; therefore, the $CO_2$ fixation amount can be calculated from the increase in $CaCO_3$ content after carbonation. The $CO_2$ fixation amount was expressed as the mass of $CO_2$ fixed per unit mass of dry carbide slag, with the unit of g $CO_2$/g carbide slag.

The $CO_2$ fixation amount was calculated as follows:

$$Uco_2 = \frac{m_{co_2}}{m_s} \tag{2}$$

Where $Uco_2$ is the $CO_2$ fixation amount, $m_{co_2}$ is the mass of $CO_2$ fixed after carbonation, and $m_s$ is the dry mass of carbide slag.

The carbonation efficiency was used to evaluate the relationship between the actual $CO_2$ fixation amount and the theoretical maximum $CO_2$ fixation amount. It was calculated as follows:

$$\eta = \frac{Uco_2}{Uco_2, max} \times 100\% \tag{3}$$

Where η is the carbonation efficiency, $Uco_2$ is the actual $CO_2$ fixation amount, and $Uco_2, max$,theo is the theoretical maximum $CO_2$ fixation amount calculated from the reactive $Ca(OH)_2$ content in carbide slag.

To further analyze the carbonation rate under different moisture contents, $CO_2$ uptake curves were plotted based on the $CO_2$ fixation amount at different reaction times. By comparing the $CO_2$ uptake of each group at 10, 30, 60, and 120 min, the effect of moisture content on the initial carbonation rate and final uptake capacity could be analyzed.

## 3 Results and Discussion

### 3.1 Effect of moisture content on $CO_2$ uptake

The variation of $CO_2$ uptake with reaction time

under different moisture contents is shown in Figure 2. Overall, the $CO_2$ uptake of all samples increased gradually with reaction time, but obvious differences were observed among samples with different moisture contents. The dry sample, namely the 0% moisture sample, showed the lowest $CO_2$ uptake throughout the reaction. Its $CO_2$ uptake was only 0.23 mol/kg at 10 min and increased to 0.90 mol/kg after 120 min. This indicates that, without additional moisture, carbide slag can still undergo a certain degree of carbonation with $CO_2$, but both the reaction rate and final uptake are relatively low.

As the moisture content increased, the $CO_2$ capture capacity of carbide slag improved markedly. At 5% moisture content, the $CO_2$ uptake increased to 1.80 mol/kg after 120 min. At 10% moisture content, the $CO_2$ uptake further increased to 2.90 mol/kg. Compared with the dry sample, the $CO_2$ uptake values of the 5% and 10% moisture samples increased by approximately 100.0% and 222.2%, respectively. This suggests that an appropriate amount of moisture can improve the carbonation conditions of carbide slag and facilitate the participation of $CO_2$ in the carbonation reaction of $Ca(OH)_2$.

When the moisture content increased to 20%, the sample exhibited the highest $CO_2$ capture capacity. The $CO_2$ uptake, $CO_2$ fixation amount, carbonation efficiency and pH values of the samples after 120 min carbonation are summarized in Table 1.

The highest uptake was obtained at 20% moisture. As summarized in Table 1, this group fixed 4.60 mol/kg after 120 min, equivalent to 0.2024 g $CO_2$/g carbide slag and a carbonation efficiency of 36.8%. The increase relative to the dry sample was approximately 411.1%. At this moisture level, water apparently supplied enough liquid phase for $CO_2$ dissolution and $Ca^{2+}$ transport while still preserving gas pathways through the particle bed.

The positive effect of water did not continue at 30% moisture. At this higher dosage, the 120 min uptake fell to 3.20 mol/kg, below the value obtained at 20%. This decrease suggests that excess water began to dominate the transport process by thickening the surface water film and occupying interparticle voids. The resulting diffusion resistance reduced the contact between incoming $CO_2$ and unreacted internal $Ca(OH)_2$. Within the range examined here, 20% moisture therefore represented the most favorable balance between reaction promotion and mass transfer.

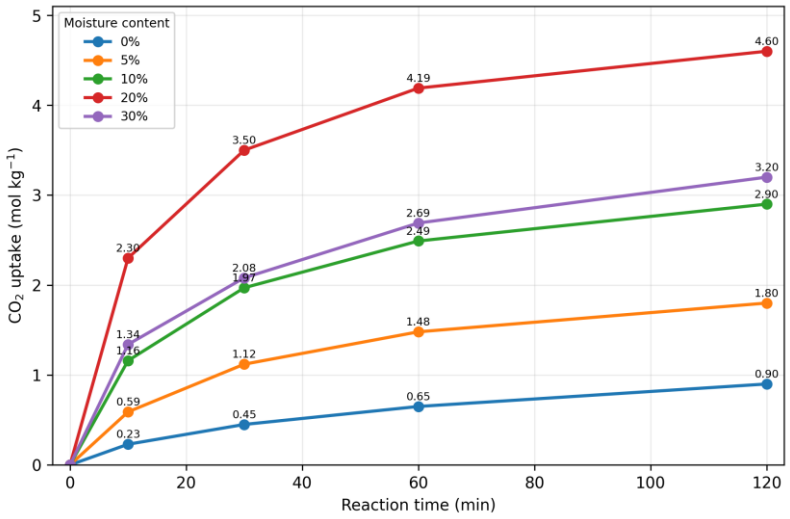


**Figure 2** Variation of $CO_2$ uptake with reaction time under different moisture contents

**Table 1** $CO_2$ capture results of carbide slag after 120 min carbonation under different moisture contents

| Moisture content/% | $CO_2$ uptake/(mol·kg$^{-1}$) | $CO_2$ fixation/(g·g$^{-1}$) | Carbonation efficiency/% | pH |
|---|---|---|---|---|
| 0 | 0.90 | 0.0396 | 7.3 | 12.15 |
| 5 | 1.80 | 0.0792 | 14.4 | 11.75 |
| 10 | 2.90 | 0.1276 | 23.2 | 11.25 |
| 20 | 4.60 | 0.2024 | 36.8 | 10.55 |
| 30 | 3.20 | 0.1408 | 26.1 | 10.95 |

### 3.2 Variation of $CO_2$ uptake with reaction time

The $CO_2$ uptake values of the samples at 10, 30, 60 and 120 min are listed in Table 2 and plotted in Figure 2. As shown in Table 2 and Figure 2, the $CO_2$ uptake of all samples increased rapidly at the early stage and then gradually approached a plateau. For the 20% moisture sample, the $CO_2$ uptake reached 2.30 mol/kg at 10 min, accounting for 50.0% of the final uptake at 120 min. At 60 min, the uptake reached 4.19 mol/kg, accounting for 91.1% of the final value. This indicates that the carbonation reaction of carbide slag mainly occurred rapidly in the early stage, and the increase in $CO_2$ uptake gradually decreased as the reaction proceeded.

This trend is related to the carbonation process of carbide slag. In the initial reaction stage, a large amount of unreacted $Ca(OH)_2$ existed on the sample surface, and $CO_2$ could easily contact the active calcium component; thus, the reaction rate was high. As carbonation proceeded, $CaCO_3$ gradually formed and deposited on particle surfaces, partially covering the unreacted $Ca(OH)_2$ and increasing the resistance for $CO_2$ diffusion into the particle interior. Therefore, the $CO_2$ uptake rate decreased in the later stage, and the curve gradually approached a plateau. Similar product-layer diffusion resistance and late-stage rate reduction have also been reported in the mineral carbonation of carbide slag and other alkaline solid wastes[20].

Moisture content also changed the initial reaction rate. At 10 min, the uptake of the dry group was only 0.23 mol/kg, whereas the 20% group reached 2.30 mol/kg. The difference indicates that suitable moisture increased not only the final capacity but also the early availability of reactive calcium. Although the 30% group remained higher than the 0%, 5%, and 10% groups throughout the test, it was consistently below the 20% group, confirming that excessive water imposed a mass-transfer penalty.

**Table 2** $CO_2$ uptake of samples with different moisture contents at different reaction times (mol $CO_2$/kg dry carbide slag)

| Moisture content/% | 10 min | 30 min | 60 min | 120 min |
|---|---|---|---|---|
| 0 | 0.23 | 0.45 | 0.65 | 0.90 |
| 5 | 0.59 | 1.12 | 1.48 | 1.80 |
| 10 | 1.16 | 1.97 | 2.49 | 2.90 |
| 20 | 2.30 | 3.50 | 4.19 | 4.60 |
| 30 | 1.34 | 2.08 | 2.69 | 3.20 |

### 3.3 TG/DTG analysis

The TG/DTG curves of raw carbide slag and the samples carbonated under different moisture contents are shown in Figure 3. During heating, the carbide slag samples mainly showed two obvious mass-loss regions. The first region appeared at approximately 350-500 ℃, which mainly corresponded to the dehydration decomposition of $Ca(OH)_2$. The second region appeared at approximately 650-850 ℃, which mainly corresponded to the decomposition of $CaCO_3$ and the release of $CO_2$. Therefore, TG/DTG results can be used to evaluate $Ca(OH)_2$ consumption and $CaCO_3$ formation before and after carbonation.

Raw carbide slag showed an obvious mass-loss peak in the range of 350-500 ℃, indicating that the sample contained a large amount of $Ca(OH)_2$. After carbonation, the mass loss in this temperature range decreased for all samples, indicating that $Ca(OH)_2$ was gradually consumed during carbonation. Meanwhile, the mass loss in the range of 650-850 ℃ increased significantly after carbonation, indicating that the $CaCO_3$ content increased and $CO_2$ was fixed as carbonate products.

The phase contents calculated from the TG results are given in Table 3. Before carbonation, the slag contained about 4.0 wt.% $CaCO_3$ and 92.0 wt.% $Ca(OH)_2$. After carbonation, $CaCO_3$ content increased to 12.5, 20.4, 29.3, 41.6, and 31.6 wt.% for the 0%, 5%, 10%, 20%, and 30% groups, respectively. The 20% group therefore had the highest $CaCO_3$ content and the lowest residual $Ca(OH)_2$ content, 48.2 wt.%, indicating the greatest degree of conversion. The lower $CaCO_3$ content at 30% moisture supports the uptake results and shows that excessive moisture reduced the effective carbonation extent.

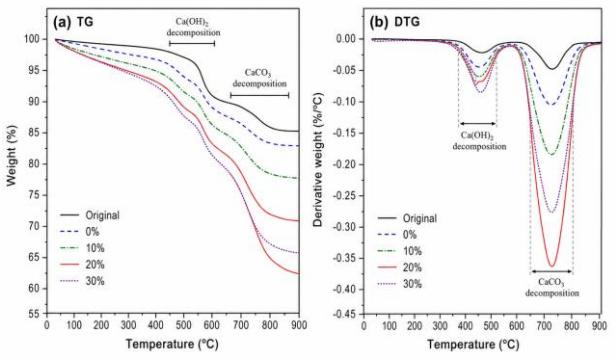


**Figure 3** TG/DTG curves of carbide slag samples before and after carbonation

**Table 3** $CaCO_3$ content and residual $Ca(OH)_2$ content of carbonated samples with different moisture contents

| Sample | $CaCO_3$ content/wt.% | Residual $Ca(OH)_2$/wt.% |
|---|---|---|
| Raw carbide slag | 4.0 | 92.0 |
| 0% | 12.5 | 82.1 |
| 5% | 20.4 | 72.9 |
| 10% | 29.3 | 62.5 |
| 20% | 41.6 | 48.2 |
| 30% | 31.6 | 59.9 |

### 3.4 XRD analysis

The XRD patterns of different samples are shown in Figure 4. The raw carbide slag showed strong characteristic peaks of $Ca(OH)_2$, indicating that $Ca(OH)_2$ was the main reactive phase in carbide slag. Weak $CaCO_3$ peaks were also observed in the raw sample, which may be related to natural carbonation during storage.

After carbonation, the characteristic peaks of $Ca(OH)_2$ decreased significantly, whereas those of $CaCO_3$ increased, indicating that $CO_2$ reacted with $Ca(OH)_2$ in carbide slag to form $CaCO_3$. As the moisture content increased from 0% to 20%, the $CaCO_3$ peak intensity gradually increased and the $Ca(OH)_2$ peak intensity gradually decreased. The 20% moisture sample exhibited the strongest $CaCO_3$ peaks, indicating that it had the highest carbonate formation, which is consistent with the TG and $CO_2$ uptake results.

When the moisture content increased to 30%, the $CaCO_3$ peak intensity was lower than that of the 20% sample, and a relatively obvious residual $Ca(OH)_2$ peak was still observed. This suggests that carbide slag was not fully carbonated under the higher moisture condition. Therefore, the XRD results further demonstrate that an appropriate amount of moisture promotes the conversion of $Ca(OH)_2$ to $CaCO_3$, while excessive moisture limits the continued carbonation reaction.

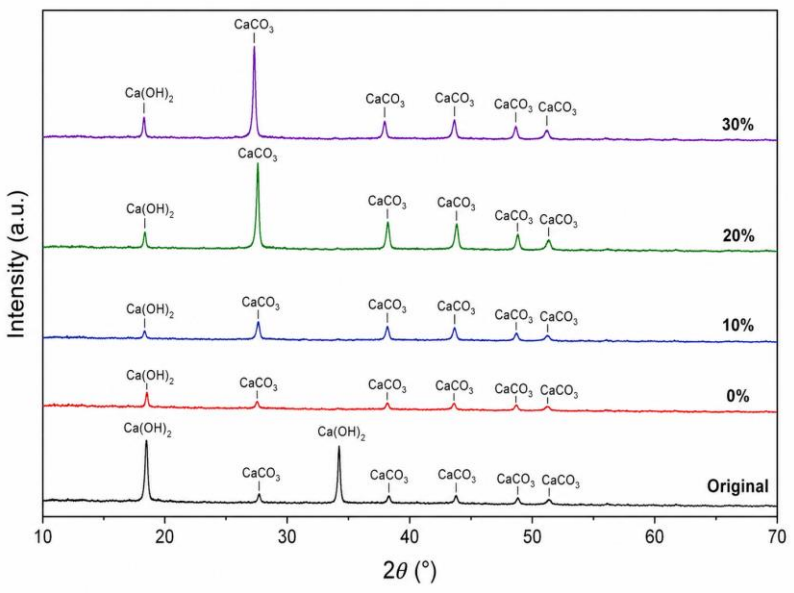


**Figure 4** XRD patterns of carbide slag samples before and after carbonation

### 3.5 FTIR analysis

Figure 5 shows the FTIR spectra of raw carbide slag and the samples carbonated under different moisture contents. An absorption peak related to -OH can be observed in the raw carbide slag, indicating the presence of $Ca(OH)_2$. After carbonation, the characteristic absorption peaks related to $CO_3^{2-}$ were significantly enhanced, indicating that $CaCO_3$ was formed during carbonation.

Specifically, the absorption peak near 1400–1500 $cm^{-1}$ was enhanced in the carbonated samples, which is mainly associated with the asymmetric stretching vibration of $CO_3^{2-}$. In addition, characteristic absorption peaks of calcium carbonate appeared or increased near 875 $cm^{-1}$ and 712 $cm^{-1}$. As the moisture content increased from 0% to 20%, the carbonate-related peaks gradually strengthened, indicating increased $CaCO_3$ formation. The carbonate peaks of the 30% moisture sample were weaker than those of the 20% sample, which is consistent with the $CO_2$ uptake, TG, and XRD results.

As an auxiliary characterization method, FTIR further confirms that $CO_2$ was fixed as carbonate products during the direct carbonation of carbide slag. Combined with XRD and TG results, the main product of the carbonation reaction can be identified as $CaCO_3$.

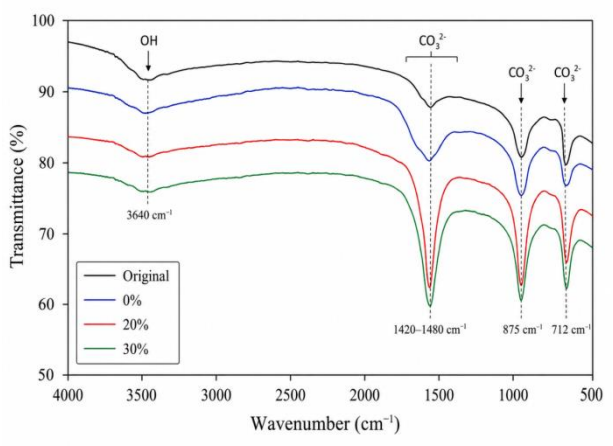


**Figure 5** FTIR spectra of carbide slag samples before and after carbonation

### 3.6 Mechanism of moisture-assisted direct carbonation of carbide slag

The combined uptake, TG/DTG, XRD, and FTIR results indicate that the effect of moisture is governed by the competition between chemical facilitation and mass-transfer resistance. Under dry conditions, the reaction is largely restricted to $Ca(OH)_2$ sites that are directly accessible to gaseous $CO_2$. Without a liquid phase, $CO_2$ dissolution is limited and $Ca^{2+}$ transport is weak, so the uptake remains low. This behavior is typical of gas-solid carbonation systems in which the reaction interface and diffusion path constrain the overall rate[8,9,21].

When limited moisture is introduced, a thin water film can form on particle surfaces and within contact zones. This film enhances $CO_2$ dissolution and supports the dissolution of $Ca(OH)_2$, producing $Ca^{2+}$ that can react with carbonate species to precipitate $CaCO_3$. The increases observed for the 5%, 10%, and especially 20% groups reflect this moisture-assisted pathway. The 20% condition appears to provide enough liquid phase for ion migration without blocking most of the gas channels in the particle bed.

At excessive moisture content, the controlling factor shifts toward gas transport. Additional water can thicken the surface film and occupy interparticle pores, which increases the resistance for $CO_2$ to penetrate into the sample and reach unreacted $Ca(OH)_2$. Although ion migration remains favorable in the water-rich environment, the supply of $CO_2$ to internal reactive sites becomes insufficient. Consequently, direct carbonation of carbide slag has an optimum moisture window rather than a simple positive dependence on water content.

Overall, carbide slag fixed $CO_2$ directly at ambient temperature and pressure, and its performance depended strongly on moisture regulation. The uptake increased from the dry condition to 20% moisture and then declined at 30%. The best result, 4.60 mol/kg after 120 min with 0.2024 g $CO_2$/g carbide slag and 36.8% carbonation efficiency, was obtained when gas diffusion and liquid-phase reaction were balanced. This finding identifies moisture control as a key operating parameter for improving carbide slag carbonation.

## 4 Conclusions

This study investigated the direct carbonation behavior of carbide slag for $CO_2$ capture under different moisture contents. The results show that the abundant $Ca(OH)_2$ in carbide slag can react with $CO_2$ to form $CaCO_3$ at ambient temperature and pressure, indicating its potential as a low-cost calcium source for $CO_2$ mineral capture. Moisture content significantly affected the carbonation performance of carbide slag, and the $CO_2$ uptake first increased and then decreased with increasing moisture content. The 20% moisture sample exhibited the best carbonation performance, with a $CO_2$ uptake of 4.60 mol/kg, a $CO_2$ fixation amount of 0.2024 g/g, and a carbonation efficiency of 36.8% after 120 min. When the moisture content increased to 30%, the $CO_2$ uptake decreased to 3.20 mol/kg.

TG/DTG, XRD, and FTIR analyses show that $Ca(OH)_2$ was gradually converted into $CaCO_3$ during carbonation, and the highest $CaCO_3$ formation occurred under the 20% moisture condition. Mechanistically, moderate moisture promoted $CO_2$ dissolution, $Ca(OH)_2$ dissolution, and $Ca^{2+}$ migration, whereas excessive moisture increased $CO_2$ diffusion resistance by thickening the water film and filling pore spaces. A suitable moisture range is therefore essential for efficient direct $CO_2$ capture by carbide slag. These results provide an experimental basis for carbonation-based utilization of alkaline industrial residues.

**Funding:** This work was supported by the Shaanxi Qinchuangyuan “Scientists and Engineers” Team Building Program (No. 2023KXJ-242), the Youth

Innovation Team Project of Shaanxi Universities (2023—2026), and the Key Scientific and Technological Innovation Team Project of Shaanxi Province.

## References

[1] WANG S, LIN X, ZHANG Y, et al. A review of utilizing carbide slag to sequestrate carbon dioxide by mineral carbonation: Mechanisms, processes, and value-added products [J]. Fuel, 2025(384): 134041.

[2] KOTHARI M S, ALY HASSAN A, EL-DIEB A, et al. Recent advancements in $CO_2$ capture and storage using carbide slag waste: a review of technological and chemical innovations [J]. Current Opinion in Chemical Engineering, 2025(49): 101169.

[3] MAZZOTTI M, ABANADES J C, ALLAM R, et al. Mineral carbonation and industrial uses of carbon dioxide [M]//IPCC Special report on carbon dioxide capture and storage. Cambridge University Press, 2005[2026-06-08].

[4] Carbon dioxide storage through mineral carbonation Nature Reviews Earth & Environment [EB]. [2026-06-08].

[5] Research on Utilizable Calcium from Calcium Carbide Slag with Different Extractors and Its Effect on $CO_2$ Mineralization [EB]. [2026-06-08].

[6] CHINDAPRASIRT P, JATURAPITAKKUL C, TANGCHIRAPAT W, et al. Carbon dioxide capture with aqueous calcium carbide residual solution for calcium carbonate synthesis and its use as an epoxy resin filler [J]. Journal of Environmental Management, 2023(345): 118783.

[7] ZHANG W, LI Y, HE Z, et al. $CO_2$ capture by carbide slag calcined under high-concentration steam and energy requirement in calcium looping conditions [J]. Applied Energy, 2017(206): 869-878.

[8] KOTHARI M S, ALY HASSAN A, EL-DIEB A, et al. Direct mineral carbonation of carbide slag waste in fixed bed reactor: comparison of dry and wet route [J]. Sustainable Environment Research, 2025, 35(1): 14.

[9] YANG J, LIU S, MA L, et al. Mechanism analysis of carbide slag capture of $CO_2$ via a gas-liquid-solid three-phase fluidization system [J]. Journal of Cleaner Production, 2021(9279): 123712.

[10] LIU Z, HOU L, LI J, et al. Efficient carbon sequestration of calcium carbide slag based on additive regulation [J]. Journal of Environmental Chemical Engineering, 2025, 13(5): 117880.

[11] GAO Y, WANG J, WEI B, et al. Understanding the mechanism of $CO_2$ mineralization and carbon sequestration performance in carbide slag: Effects of liquid-solid ratio and gas flow rate [J]. Journal of Environmental Management, 2025(390): 126246.

[12] Effect of Wet Carbonation of Calcium Carbide Slag on $CO_2$ Sequestration and the Prevention of Coal Spontaneous Combustion ACS Omega [EB]. [2026-06-08].

[13] LU H, WANG W, ZHANG J, et al. Accelerated Direct Mineralization of $CO_2$ by Carbide Slag under Ambient Temperature and Pressure Reaction Conditions [J]. Energy & Fuels, 2024, 38(15): 14483-14492.

[14] GONG W, SHEN P, TANG Y, et al. A review in calcium carbide slag utilization for carbonation: from methods to applications [J]. Cleaner Materials, 2026(19): 100374.

[15] KOTHARI M S, ALY HASSAN A, EL-DIEB A, et al. Modelling and optimization of carbon dioxide sequestration potential of carbide slag waste [J]. Case Studies in Chemical and Environmental Engineering, 2025(12): 101250.

[16] Steam Efficiently Enhancing $CO_2$ Direct Mineralization Steel Slag Towards Actual Production: Phase Evolution, Microstructure, and Mechanisms [EB]. [2026-06-08].

[17] Exploring the Effect of Moisture on $CO_2$ Diffusion and Particle Cementation in Carbonated Steel Slag [EB]. [2026-06-08].

[18] XU Q, GAO Z, ZHANG D, et al. The Characterization of Carbide Slag by Carbonation Curing and Its Enhancement Performance in Blended Cement Paste [J]. Journal of Materials in Civil Engineering, 2024, 36(1): 04023504.

[19] Sustainable $CO_2$ utilization and calcium carbonate recovery from calcium carbide wastewater: iScience [EB]. [2026-06-08].

[20] Research progress of steel slag-based carbon sequestration - ScienceDirect [EB]. [2026-06-08].

[21] Mineral $CO_2$ Sequestration by Steel Slag Carbonation Environmental Science & Technology [EB]. [2026-06-08].

Publisher: Viser Technology Pte. Ltd.

URL: www.viserdata.com

Add.:195 Pearl's Hill Terrace, #02-41,

Singapore 168976

ISSN 2661-4456

01